SCATTEROMETRY

David L.T. Anderson
Dept. of Atmospheric, Oceanic and Planetary Physics
Oxford University

ABSTRACT

A scatterometer is an instrument capable of providing high resolution measurements of the wind velocity near to the surface of the ocean. There are difficulties in using this data however. Firstly it is not unambiguous: a unique wind direction is not generally obtained, so methods of selecting the true direction from among the several possible must be developed. Experience of objective ambiguity-removal techniques using simulated ERS-1 data is reported.

A second difficulty is that of obtaining impact from using this single-level boundary layer data. To examine this aspect, manually dealiased data from SASS is used in the ECMWF analysis forecast model. In addition comparison is made between the SASS data and the analysed fields as well as with other data used in the analysis.

1. Introduction

The lack of adequate wind observations over the world's oceans has long been noted as a serious handicap for those trying to model the ocean circulation, as well as those trying to forecast the weather. It is expected that new satellites carrying scatterometers to measure the near-surface wind will be launched within the next few years. One must therefore begin to adapt meteorological models to extract the maximum information from these measurements both for the benefit of weather forecasting and ocean modelling. The data is not likely to be easy to use in meteorological models as it is single level boundary layer data. Its use will be further complicated by the fact that the wind direction is not uniquely determined.

A scatterometer is an active instrument in that a pulse of radiation is emitted, and a measure made of the amount returned from the sea surface. Typical wavelengths of the radiation are a few centimeters. The full physics of the scattering process at

the sea surface are not well understood but Bragg scattering may give the dominant contribution. In general, a unique solution is not obtained for the wind velocity, giving rise to one of the major problems in using scatterometer data. In fact, up to four wind directions are possible, depending on the number of antennae. The process of selecting the correct solution from the possible choices is frequently called ambiguity removal or dealiasing (although the choices or 'aliases' are not really aliases in the normal sense). Having obtained a unique solution, one can then use this data, for example assimilating it into a meteorological analysis forecast model.†

As a step in the development programme, the experience of using scatterometer data in the ECMWF analysis-forecast model is reported. Because no real data from the planned scatterometer instruments (such as the one to be carried on ERS-1) exists, it was decided to use data from the SASS scatterometer, carried on the SEASAT satellite, which is still the only satellite-borne scatterometer to date. It operated for some 3 months but only data for a short period towards the end of the mission (6–17 September 1978) is considered here. The next scatterometer will be carried by the ERS-1 satellite with another, NSCATT to follow probably a year or two later. Although the instruments differ in design somewhat, the principle of operation is similar.

In section 2 the physical principle on which the scatterometer is based will be discussed, together with the origin and nature of the multiple solutions. Because the volume of data returned by the instrument is quite large it is unlikely that the selection of a wind direction from the several possible can be done subjectively. Rather methods which do not in general depend on human intervention must be developed. Tests of ambiguity removal methods using simulated data are described in section 3. In section 4, results of using scatterometer data in a model equivalent to the ECMWF analysis-forecast model are described.

2. How a scatterometer works

Because the theory relating the backscattered radiation (a normalised version of which is usually called sigma naught, and denoted σ^o) to sea surface conditions is not well understood, an empirical relationship is used instead, based on observed correlations between surface wind speed and σ^o. To keep the argument simple, let us assume the

† *One could use the raw data in other ways, and combine the dealiasing and analysis/assimilation into one process.*

main process is Bragg scattering as indicated in fig. 1. The argument as to how a scatterometer works is that the incoming radiation will be scattered primarily by ripples with a wavelength comparable to that of the incoming radiation. These ripples or waves are rather short and one might think that they would respond quickly to the wind and saturate i.e. if the wind amplitude increased, these small waves would not get any bigger. If this was all that was at work, a scatterometer could not sense wind speed, since the amplitude of the ripples would be largely independent of the wind speed. In fact, the above picture is not correct, since the little waves ride on bigger waves which are not independent of wind speed, and the wave spectrum of short waves, although difficult to measure is now not thought to saturate. (Phillips 1985). Further, since the scatterometer has a field of view (footprint) covering many square kilometers the fraction of that area covered instantaneously by the ripples may be a function of wind speed. Whatever the physics, there is plenty of evidence that σ^o increases with increasing wind speed, at least until wind speeds of over 20m/s. There may be a low wind speed cut-off at ~ 2 ms^{-1}, below which no meaningful wind direction is obtainable.

The reader will note that there is a wishwash of ideas between wind speed, sea state and σ^o in the above. In reality, σ^o is likely to be most closely related to sea state, but this is not the variable one wants to measure: wind velocity or wind stress is more interesting. Although the sea state may respond rapidly to the wind at short wavelength, at longer wave lengths, the response need not be local. To the extent that non-local swell waves influence the return signal, it may not be possible to use a local relationship between wind velocity and σ^o measurements. It may be that a forecast of the wave state, based on previous knowledge of the wind state will also be required. This remains an open question, and at ECMWF steps are in progress to implement a wave model which can be used to improve the σ^o inversion process. Be that as it may, non-local effects are not, in general, dominant and for the moment we will assume a local response.

The ability to detect wind direction comes from the fact that the σ^o response is small when the short waves (and hence the wind) are at right angles to the emitted pulse, and larger when the short waves (and wind) are aligned with the emitted pulse. So σ^o will be a function of wind direction as well as wind speed. It is also a function of

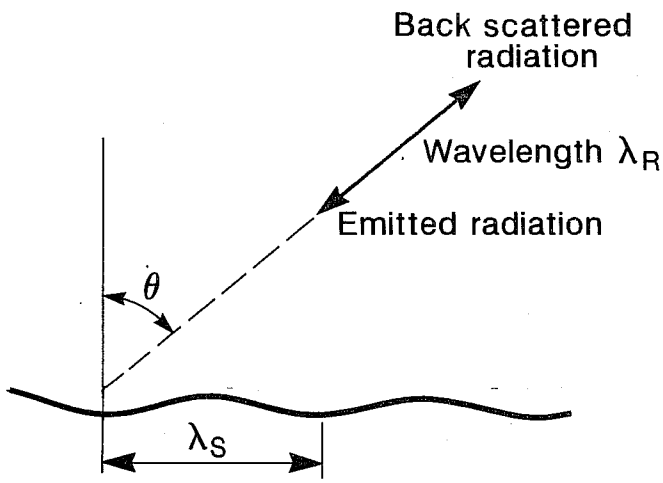

Fig. 1a:

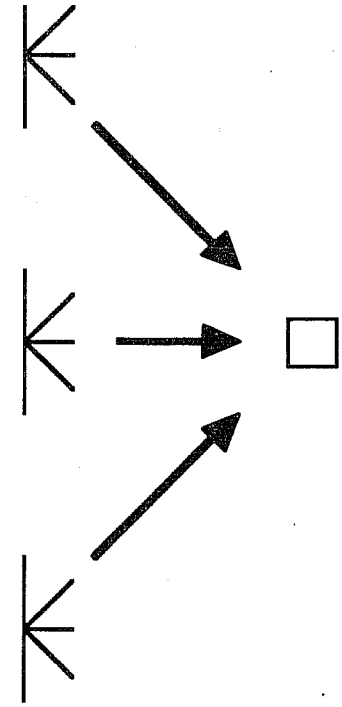

Fig. 1b:

Fig. 1a: Bragg scattering geometry. The wavelength of the ocean waves involved in the scattering processes, λ_s, is related to the wavelength of the emitted waves λ_R by $\lambda_s = \frac{\lambda_R}{2\sin\theta}$ where θ is the angle between the radar viewing direction and the normal to the ocean surface. For SASS, the ocean wavelengths were ~2 cms: for ERS1 they will be longer typically 5 cms.

Fig. 1b: A patch of ocean is viewed as the satellite approaches by the forward beam, and as it recedes by the rear beam. This was the configuration for Seasat. For ERS1 the patch will also be viewed by a central antenna as the satellite passes by. Seasat viewed to both sides but ERS-1 will view only to one side as illustrated.

the incidence angle, θ, shown on fig. 1, giving

$$\sigma^o = f(V, \varphi, \theta) \tag{1}$$

where V is the wind speed, φ is the angle between the wind direction and the antenna beam and θ the incidence angle.

As noted above, the functional relationship (1) is not derived from theory. Rather, one flies a scatterometer in an aircraft over the sea and measures the value of σ^o for various incidence angles. In conjunction with the aircraft measurements, ships record the wind speed and direction. An empirical functional relationship between σ^o and wind speed, direction and incidence angle is then sought. The mode of operation is to mount the scatterometer on a satellite, measure σ^o and then invert (1) to obtain wind speed and direction (θ is taken as known). The patch which is illuminated by the beam is several kilometers square. For ERS-1, for example, an inversion is expected for boxes 25km square lying within a swath extending from approximately 250km to 700km from the subsatellite track. (The instrument does not work well at low incidence angles, nor at too high incidence angles).

For one measurement of σ^o, eqn (1) cannot be uniquely inverted for two pieces of information (V, φ). One might anticipate two measurements of σ^o would be necessary, but this is in fact insufficient as fig. 2 shows. Plotted, are the values of V and φ for a given σ^o and given incidence angle. If one has 2 measurements of the same patch of ocean, one from a forward and one from a rear look as in fig. 1 then there are 4 possible intersections. This is the source of the ambiguity referred to above. If more beams are added then this ambiguity can be reduced and we will consider this now, mainly within the framework of ERS-1. [NSCATT will use a somewhat different method of increasing the number of independent pieces of information by including measurements obtained when the emitted radiation is either vertically or horizontally polarised as well as from three beams, but we will not discuss this further].

The ERS-1 scatterometer will measure the backscattered radiation σ_i^o from three beams, σ_1^o from a forward, σ_2^o from mid beam and σ_3^o from a rear beam as in fig. 1. The particular model function used to relate backscatter to the wind speed at 10m and wind direction relative to the antenna beam φ_i is known as CMOD1 (Long 1986). The model function is likely to depend on parameters other than just V, φ and θ (e.g. ocean surface conditions such as surfactants, boundary layer stability, sea surface temperature, non

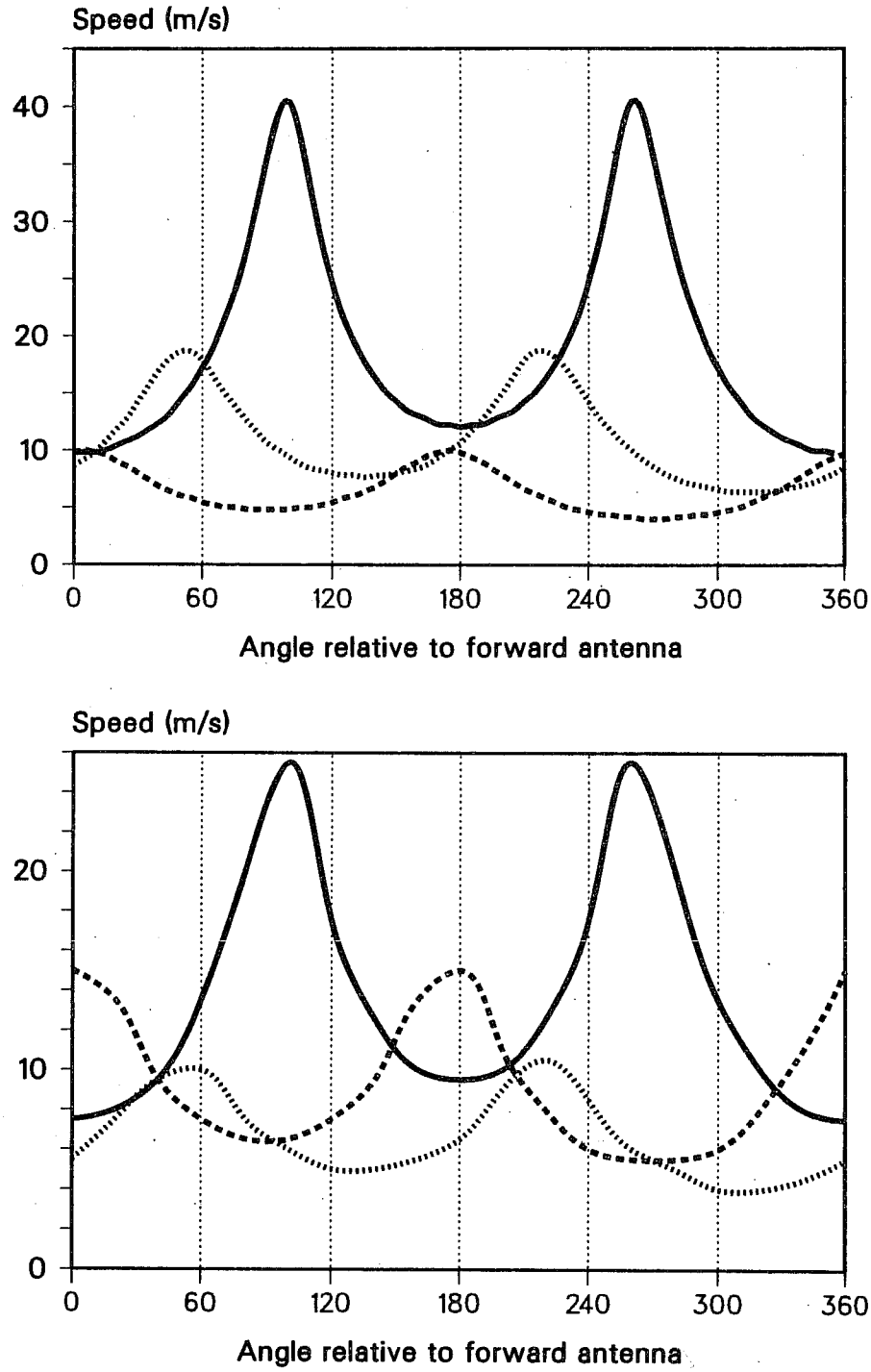

Fig. 2: Sketch of possible (v, ϕ) curves for a single value of σ^o from the forward beam (solid), rear beam (dashed) and central beam (dotted), for a wind direction at 40° to the forward beam. If there is no central beam, the curves intersect in 4 possible locations giving rise to 4 aliases, all with much the same speed but quite different directions. In the presence of a third beam there is only 1 common intersection of the 3 curves, but if there is noise on the measurements of σ^o, the curves will be displaced and there will in general be no common intersection of all 3 curves.

local wave response). Further, being deduced from only a limited number of ground campaign studies, the empirical relation given by (1) is itself likely to be less than perfectly described. But for the purpose of this section it will be taken as correct and model function error not considered further.

With a 3 beam instrument such as ERS-1, we have three pieces of information to determine 2 unknowns (V,φ) (where φ without a subscript will from now on be used to denote wind speed measured relative to the space craft direction). As is common in over-determined problems, a solution is sought in (V,φ) space to minimise some function. For ERS-1, the functional form presently being considered is

$$F_1\ (v,\varphi)\ = \left[\frac{(\sigma_1 - \hat{\sigma}_2)}{KP_1\ \hat{\sigma}_1}\right]^2 + \left[\frac{(\sigma_2 - \hat{\sigma}_2)}{KP_2\ \hat{\sigma}_2}\right]^2 + \left[\frac{(\sigma_3 - \hat{\sigma}_3)}{KP_3\ \hat{\sigma}_3}\right]^2 \qquad (2)$$

where KP is a measure of the noise on the measurement and $\hat{\sigma}$ indicates the value of σ obtained from the model function for the trial speed and direction φ, and σ the measured value.

The problem of finding solutions to (1) now reduces to finding values of (V,φ) which correspond to minima of (2) and fig. 3a shows the topography of F for two different wind directions, (i) 30° and (ii) 60°. One can see that in the former case, the true solution corresponding to a minimum in F is well defined. In the latter, it is poorly defined. In fact, there are two directions which have a value of F near zero and hence the solution is still undetermined in this case even though there are measurements of σ^o from three beams. Other forms of normalising F are possible. The particular form (2) is pleasing to statisticians since it is a maximum likelihood estimator, but different normalisations can give rise to a function F which has less structure. This is illustrated in fig. 3iii, iv and v which show contours of F for a wind direction of 90° for 3 different choices of F. Panel iii is for F defined as in (2), whereas panel iv corresponds to using σ in the denominator of (2) instead of $\hat{\sigma}$ and panel v to no normalisation at all. In all cases the cell is located roughly mid-way across the swath. Based on fig. 3, one can see that in general the solution is unique, (except at certain wind directions such as 60° when it is genuinely indeterminate). Fig. 3a however corresponds to a perfect situation in which there is no noise in the measurements of σ. In practice this will not be so. The presence of noise (equivalent to moving the curves of fig. 2 up or down) can lead to a switching of solution such that the true solution may no longer be the one with the lowest value of F or, more to the point, that the lowest value of F may no longer

Fig. 3a: Contours of F for various normalisations and different wind velocities. The radial distance is a measure of the speed and the angular displacement from zero at North, a measure of the wind direction. The value of the function is scaled by a factor of 0.1. The contour interval is 0.5 where the value of the function is less than 6 and 2 elsewhere. Contours greater than 20 are not plotted. The wind speed is 10 ms^{-1}. In (i) the wind direction is 30° while in (ii) it is 60°. The absolute minimum in all panels should be zero but because the minima are only interpolated by a contouring package are not quite zero. In the case of a wind direction of 30° the magnitude of F at the secondary minimum is well distinguished from the primary minimum but when the direction is 60° the value of the secondary minimum is also very close to zero. This means that it would be very difficult to distinguish the true direction from its alias if the wind direction were 60°, but this should be skillfully done when the wind direction is 30°. In (iii), (iv) and (v) the wind direction is 90°. Three different normalisations of F are used. For (iii), the normalisation is as given in (2). For (iv), the measured σ^o is used instead of the value of σ^o for the trial wind velocity in the denominator of (2) while for (v) no normalisation at all is used. The topography of F is considerably more complicated in (iii) with 6 minima compared with only 2 in (v). The location of the two principal minima is essentially the same for all three normalisations however.

Fig. 3b: A plot of the magnitude of the values of F of the secondary minimum for different wind directions. In all cases the speed is 10 ms^{-1}. The three curves correspond to a point at the inside edge of the swath (node 1), a point in the middle of the swath (node 10) and a point at the outside edge of the swath (node 19). This figure shows clearly the directions in which skill may be expected as well as those near 60°, 120°, 190°, 240°, 300° and 350° for which the skill will be small.

Fig. 3c: Plot of the number of occasions when the rank 1, rank 2 or rank 3 solutions are correct as a function of cell position across the swath for 3 wind directions. In all 3 cases, the rank 3 solution is almost never correct. The number of times rank 1 corresponds to the true direction increases across the swath to a maximum at the outside edge. There is no skill for a wind direction of 60°, since the rank 2 solution is correct as often as the rank 1 solution. (In fact slightly more often!). Noise was added to the σ^o values before inversion.

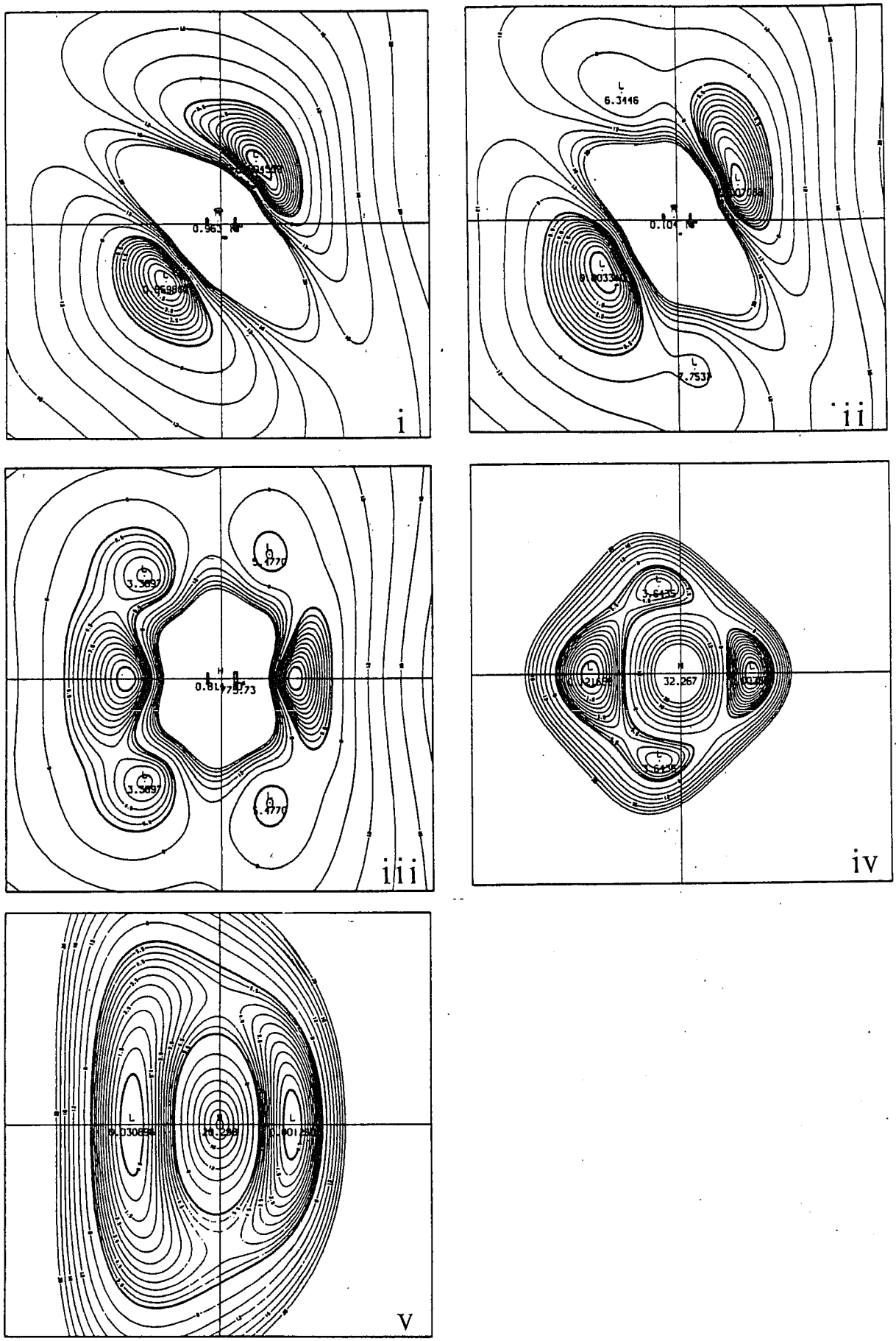

Fig. 3a:

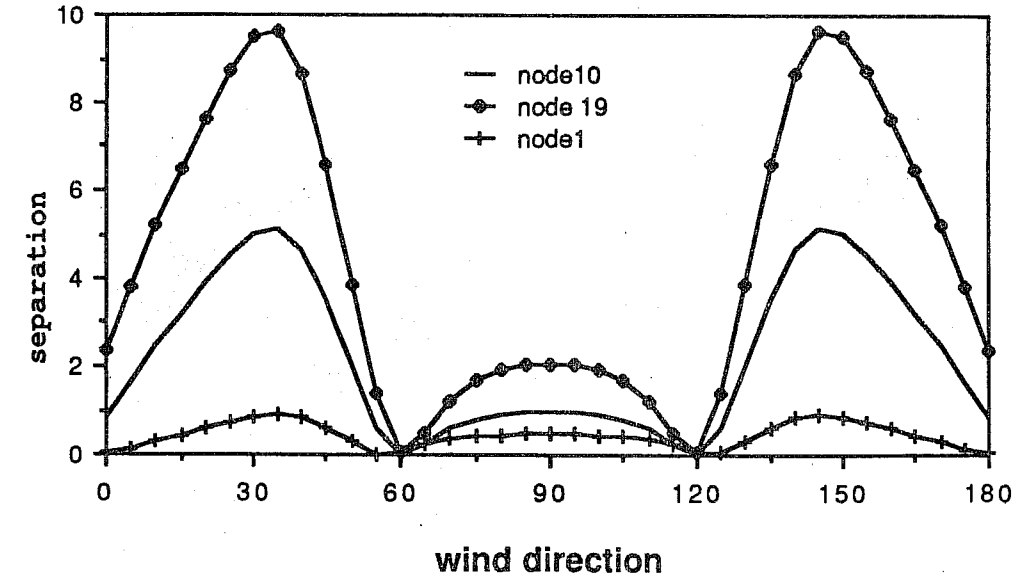
node10
node 19
node1
separation
wind direction

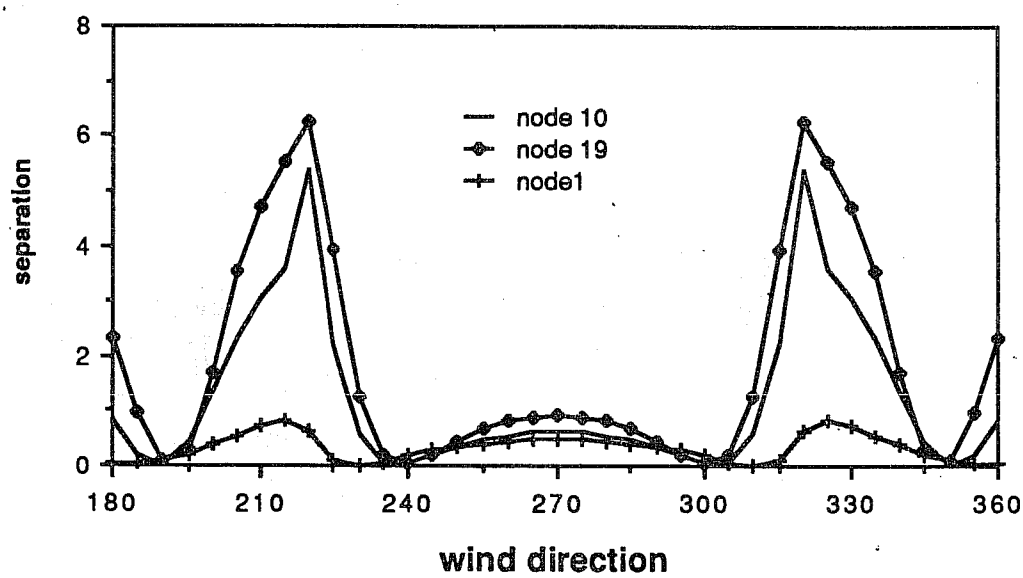
node 10
node 19
node1
separation
wind direction

Fig. 3b:

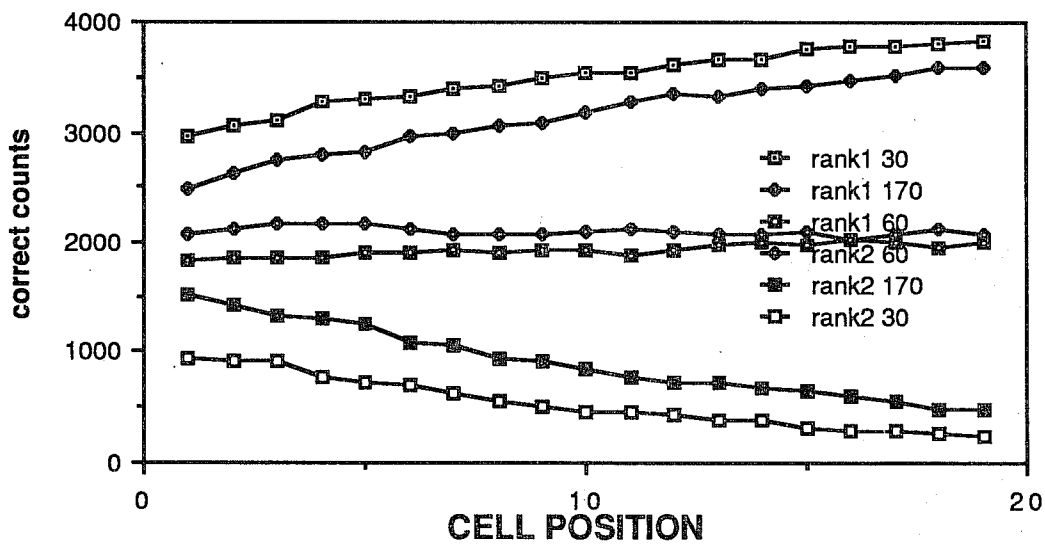
rank1 30
rank1 170
rank1 60
rank2 60
rank2 170
rank2 30
correct counts
CELL POSITION

Fig. 3c:

necessarily correspond to the true solution. Although the ordering of the minima may be switched because of noise, we still expect to be dealing with mainly a 180° ambiguity and this gives rise to the hope that the ambiguities can be removed objectively i.e. without human intervention.

The location of a cell across the swath is however relevant and this is clearly illustrated in fig. 3b which shows the depth of the second minimum in F. (The depth of the first is zero) as a function of wind direction for a wind speed of 10 ms^{-1}. If the wind is blowing from a direction approximately 60°, 120°, 195°, 240°, 300° or 345° measured clockwise from the satellite pointing direction, even with three measurements of σ^o, one can not determine the direction of the wind unambiguously. Between these 'bad' angles, there are corresponding good angles, but some good angles are better than others. (The larger the separation of the minima the better). Fig. 3b also shows a strong cross swath variation in the depth of the minima and hence in the anticipated skill, with the skill being least at the inside edge.

Fig. 3(a) and (b) were prepared without noise on the σ's. When noise is included on the σ^o measurements, then we anticipate the possibility that the wind directions corresponding to the minima in F can be switched, but the larger the value of the separation on fig. 3b, the less such switching will occur. This is confirmed in fig. 3c where the number of times the rank 1, rank 2 and rank 3 solutions is correct is plotted for 3 wind directions – a good direction (30°), a bad direction (60°) and a neither especially good nor bad direction (170°). As expected, for a wind direction of 60° the number of times the rank 1 is correct is about the same as the number of times rank 2 is correct. (Actually slightly less!). By contrast, at a direction of 30° the rank 1 almost always corresponds to the correct direction at the outside of the swath but only in about 75% of the time at the inside of the swath.

If only two beams are operational (as may happen even with a three beam instrument near land) or because the instrument is only two beam, as in the case of SASS, then the problem is much more difficult. In general there will be 4 solutions for each of which F will be zero. [In decreasing likelihood, there can be cases when there are 3 or 2 or even a unique solution if the wind is parallel to one of the beams, but the norm is 4].

For SASS, which was a two beam (fore and aft) instrument, one way of tackling the problem of removing ambiguity was to rely heavily on the analyst's ability to recognise

meteorological patterns or by choosing a direction in accord with external information such as cloud patterns or ship reports etc. To illustrate the manual process and the magnitude of the task, consider fig. 4. This is a figure from Woiceshyn *et al.*, 1987 which shows, for a small area in the South Atlantic, all the possible solutions. The task is to pick the true solution. This is done by applying meteorological principles, some concepts of smoothness and, where possible, relating the fields to independent measurements such as from ships or satellite cloud imagery etc.

Only about a 2 week period in September 1978 was manually dealiased by this method although it is now 10 years since the data was collected. To give some idea of the enormity of the task, there are almost 400,000 measurements in that 2 week period. We will discuss this data set further in section 4 as it was used as a trial dataset for assimilation in the ECMWF analysis/forecast model. Before doing so, however, we will consider how successfully we can remove the ambiguities objectively for a three beam instrument – the only practical way of handling the huge data sets from ERS-1.

3. Objective ambiguity removal

There is no unique way of objectively removing the ambiguity. One can try to utilise the fact that in certain directions the solutions are rather well separated (e.g. fig. 3a(i) for a wind direction of 30°). This would suggest, that even in the presence of noise, that the solution for 30° should be quite well determined (fig.3c). On the other hand, as fig. 3c also shows, there is no skill at angles of 60°. This is illustrated in fig. 5 where the skill is plotted as a function of incidence angle across the swath for 3 different directions, 30°, 60° and 170°. Not only does fig. 5 indicate that there is different skill for different wind directions it illustrates that there is a substantial cross-swath variation in skill.

One method of objective dealising, denoted CREO, was developed under contract to ESA, by Cavanie and Lecomte. It uses the idea of good wind directions but not explicitly the cross-swath variation in skill. Swath position is partly taken into account, however, by always processing from high incidence angles where the skill is higher, to low incidence angles where the skill is lower. The basis of the CREO algorithm is to construct two fields, which should be more or less orthogonal to each other. The first field is produced starting from the rank 1 (the solution with the lowest value of F) at the outside of the swath and then processing cell by cell to the inside edge of the swath

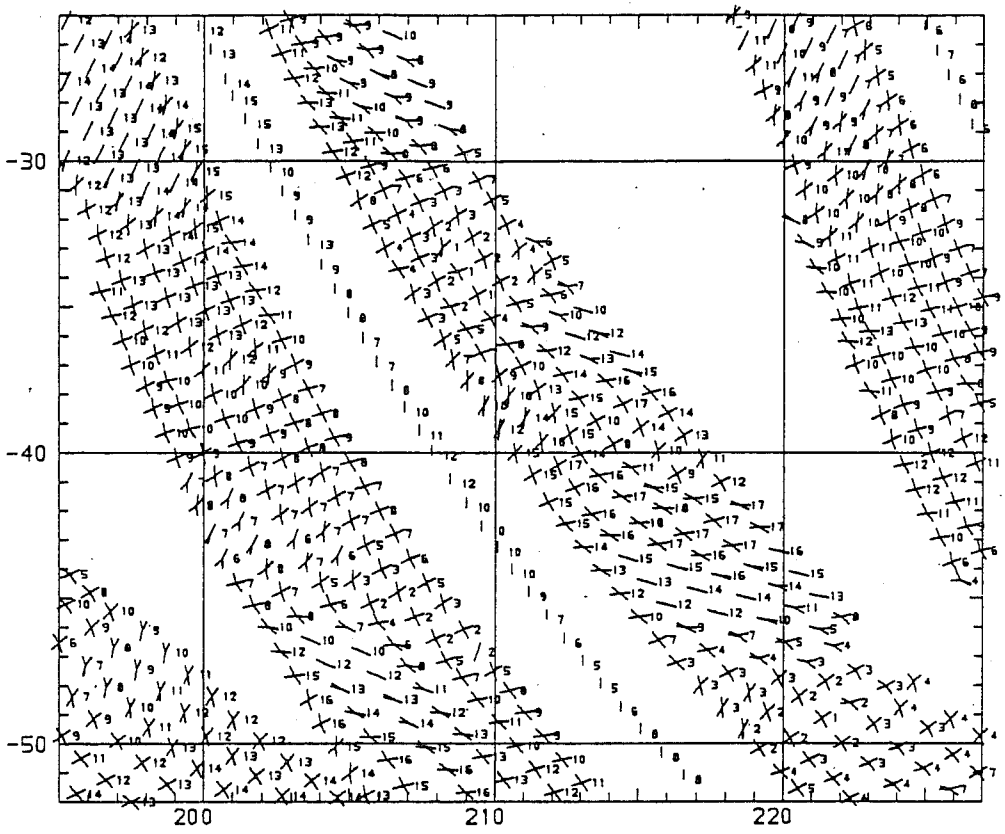

Fig. 4: Raw retrieved SASS data – swath (Rev 1048) showing multiple wind directions. 2 direction cases occur when the wind is blowing parallel to one of the beams and 4 vector solutions separated by $\sim$ 90° when the wind is blowing orthogonal to the satellite track. From Woiceshyn *et al.* 1986.

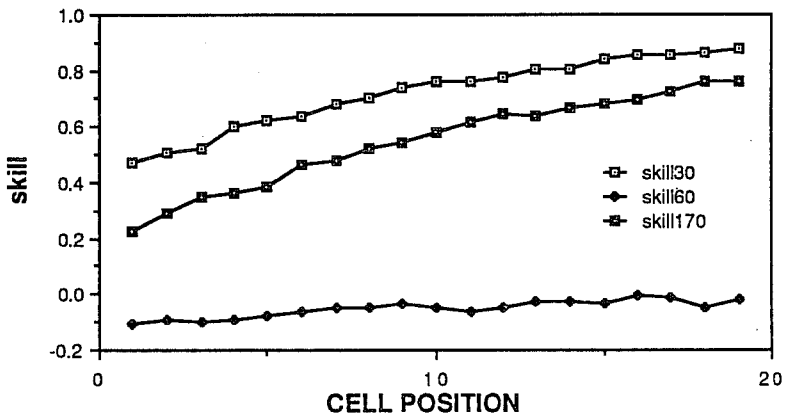

Fig. 5: Plot of the skill of the rank 1 solutions as a function of swath position for three different wind directions (30°, 60° and 170°), showing the variation in skill with respect to position across the swath as well as with wind direction. Skill is defined as $$S = \frac{R_1 - R_2 - R_3}{R_1 + R_2 + R_3}$$ where R_1 is the number of times rank 1 is correct etc. For any cell location a large number of realisations is used, each differing as a result of noise on the σ^o triplets.

picking at each cell the solution whose direction is closest to that of the preceeding two, so producing a relatively smooth field. A second field is then constructed starting with the rank 2 solution. Of the two fields so produced, the one with the highest number of rank 1 solutions in certain windows is chosen. The windows are direction bands centred on those directions for which the wind is likely to be well determined. The procedure scans over segments 2,850km long, with overlap between segments to give continuity across segment boundaries.

There are times when the algorithm does not produce solutions in which it is confident. This can occur for example if the wind is coming from one of the poor directions. If this happens over a large enough area of the swath, there will no be grounds for choosing one field over another, for, as we have seen, there is little or no skill in the ranking close to those directions. Other more elaborate tests are made as well but we do not have space to detail these here. Extensive testing of the CREO algorithm on ECMWF fields has been carried out by Graham, Anderson, Hollingsworth and Bottger (1988) and the interested reader is referred to that work and to the works of Cavanié and Lecomte referenced therein for further information. Here we will only give some flavour of the success of such an algorithm.

Fig. 6a shows a global 10m wind analysis for 13th June 1985. This field is taken as 'truth' and the satellite flown over it for about 7 hours, sweeping out the orbits shown in fig. 6b. Triplets of values of σ^o are simulated every 25km, at distances between 200km and 650km from the subsatellite track. In fig. 6c, the ability of the CREO algorithm to dealiase the σ^o in autonomous mode (i.e. without relying on external information) is illustrated. This figure is intended to show areas where, for one reason or another, the ambiguity-removal software has experienced difficulties. Regions along the tracks defined in fig. 6b which are blank in fig.6c are regions where the solution has been found correctly. This 'correct' solution will not of course be exactly correct, because the σ^o measurements will in reality be noisy (and this noise is simulated). So the retrieved wind speeds and directions will differ somewhat from those we used to produce the $\sigma^{o's}$. Typical errors in directions as a result of noise are generally less than 20°. If the ambiguity-removal software returns a direction which is more than 90° away from the true direction, this usually indicates that a wrong direction was selected by the ambiguity removal procedure. So fig. 6c, in which only solutions differing by more than 90° from the true solution are plotted, can be interpreted as giving a measure of the

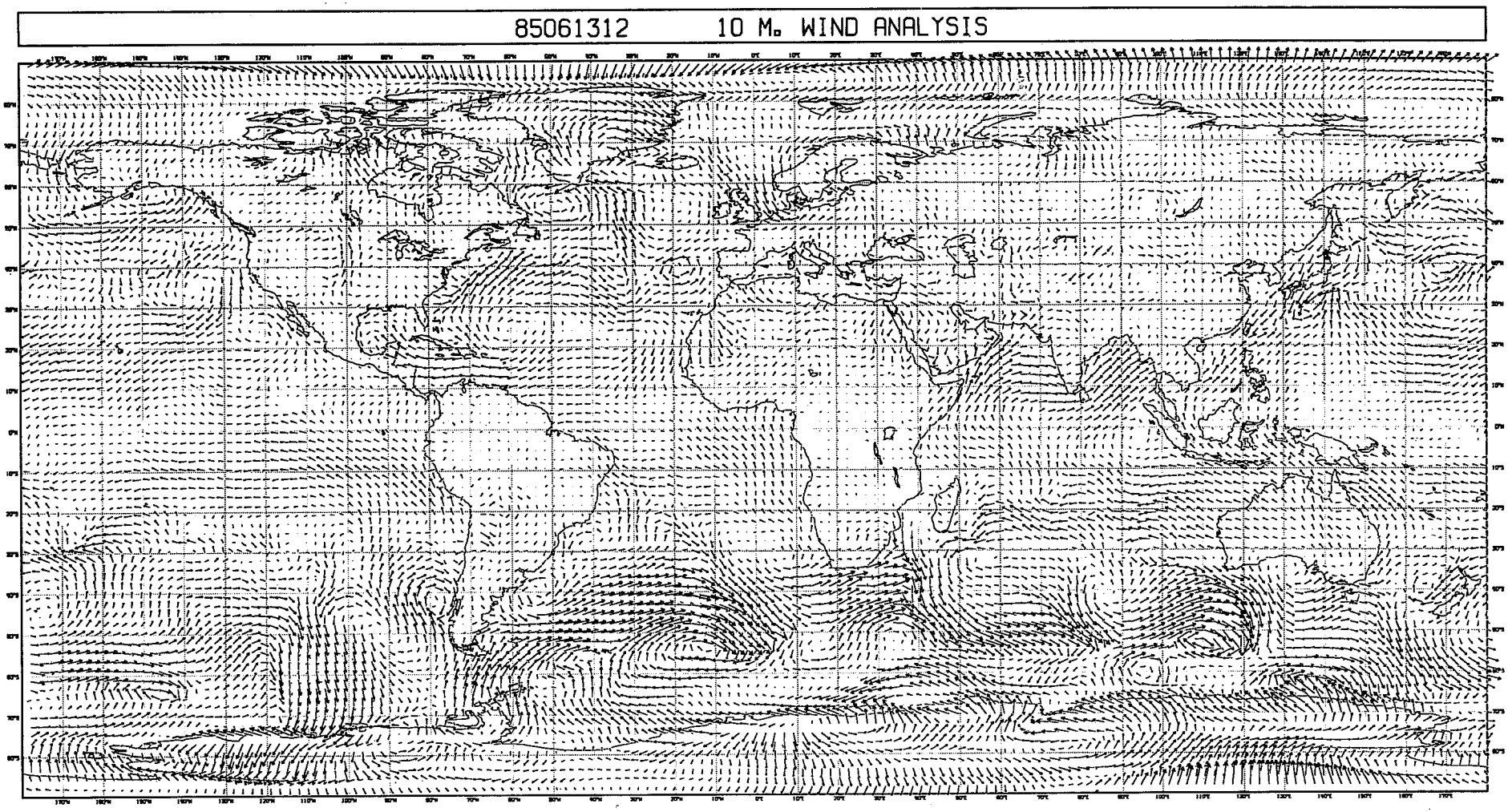

Fig. 6a: 10 m wind analysis for 12UT 13th June 1985.

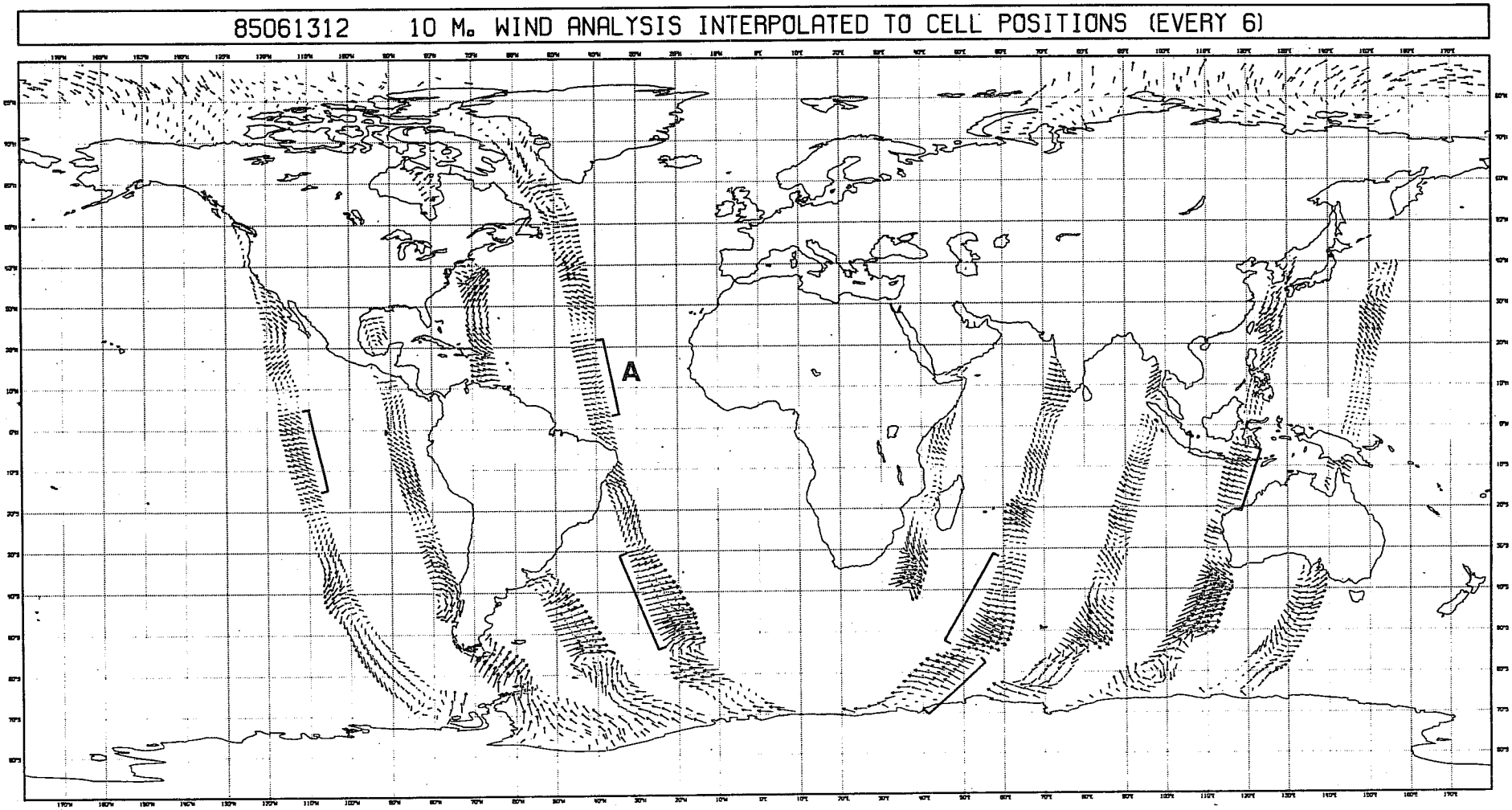

Fig. 6b: Orbits covered in a simulated 7 hour period by ERS-1. For clarity, only every 6th wind vector is plotted.

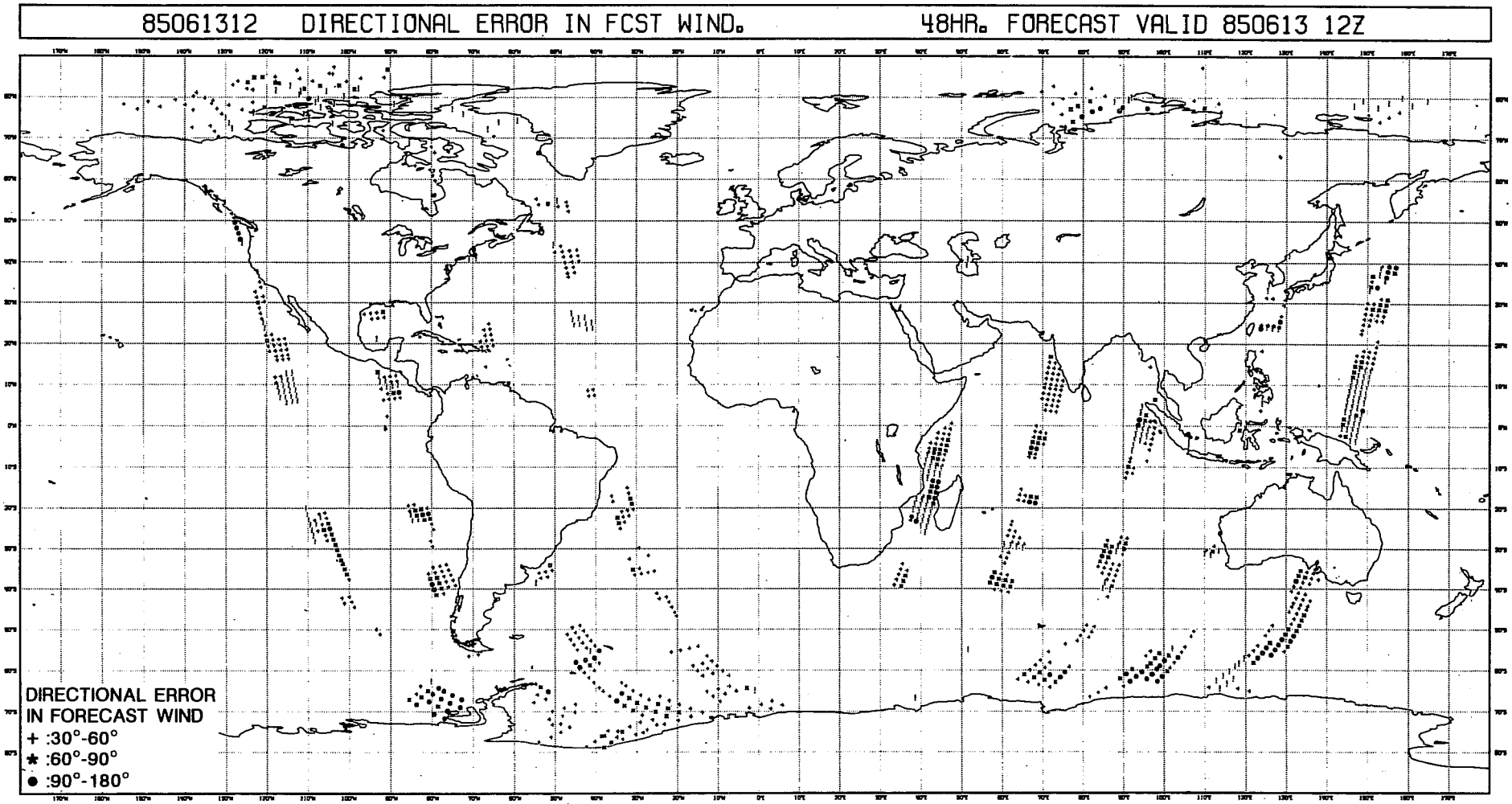

Fig. 6c: Direction error in the 48 hour forecast wind. Errors less than 30° are not plotted. Those winds which are in error by between 30° and 60° are indicated by a +, between 60° and 90° by a * and by between 90° and 180° by a •.

skill of the ambiguity-removal software. (For clarity, only every 6th solution along and across the swath is plotted).

Different codes are used to indicate different reasons for lack of confidence by the ambiguity removal software. First, as indicated earlier, the scatterometer will only work down to some minimum wind speed. For ERS-1, this is specified as $4ms^{-1}$, but in fact the instrument may work to speeds below this. Low wind areas ($<2.25ms^{-1}$) are marked on fig. 6c by a code 1. Since this inability to determine the direction is a consequence of scatterometer physics, and not of the dealiasing software, code 1 does not really indicate an error. The other areas do however indicate an inability of the ambiguity removal software to return a solution in which there is confidence. The reader will also note 5 boxes containing numbers [17, 43, 100, 2, 95]. These indicate areas where the ambiguity removal algorithm has chosen (confidently) the wrong direction. The number of 17 would correspond to roughly a whole row in error or an area of $\sim$100km square. The conclusion from fig. 6c, which is typical, is that the algorithm is accurate but conservative; there are very few wrong solutions chosen but there is an unacceptably–large number of cells for which no dealiased solution is returned. What to do? To remove the uncertainty some additional external information is required. This could be from a number of sources, such as ships, satellite cloud patterns etc but in terms of the operation envisaged for ERS-1 fast delivery product, it would take too long to assemble this information and time is of the essence. The concept of a fast delivery product is that it should be available from the ESA ground stations within 3 hours of data collection. In addition to the time constraint, only limited computing resources are available at the ground stations. A meteorological forecast field can be made available fairly easily however.

Let us now consider supplying a 48 hour forecast to the ambiguity removal algorithm. The choice of 48 hr is somewhat arbitrary. In practice, a shorter range forecast could be used, but since the analysis and forecast used in this simulation came from the same stable, 48 hrs was chosen so as not to give too over-optimistic a scenario. The present concept of global forecasting is that the forecasts are more accurate on large scales than on small, so one should try to use large-scale information in the ambiguity removal software. The scheme is now as follows. First try to dealias the data autonomously (i.e. as for fig. 6c). In areas in which confidence is low, make a check between the two opposing fields referred to earlier and the meteorological first guess

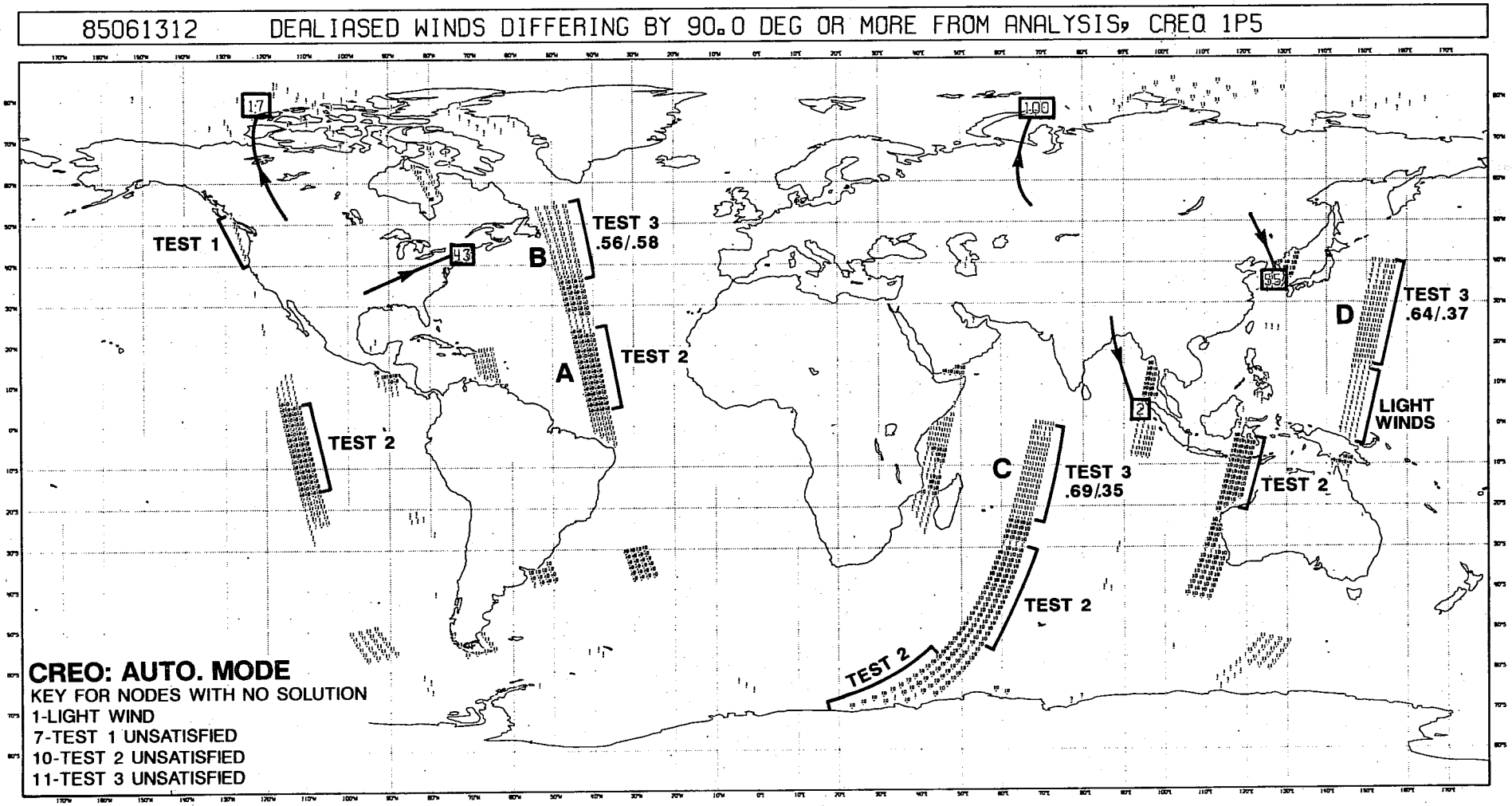

Fig. 6d: Non returns from the CREO ambiguity retrieval algorithm when used in purely autonomous mode (i.e. is not supplied with external data such as a short range weather forecast). The square boxes indicate regions where the wrong solution is selected and the figures give the number of cells which are wrong. There are only 5 boxes for which the number of errors is 17, 43, 100, 2 and 55. Where the winds are light ($<2.25 ms^{-1}$), no ambiguity removal is attempted. These regions are denoted by a 1. The other regions are areas where the software was not confident that it could dealias the solution correctly so flags were set. These indicate the reason for the uncertainty but this is beyond the scope of this paper.

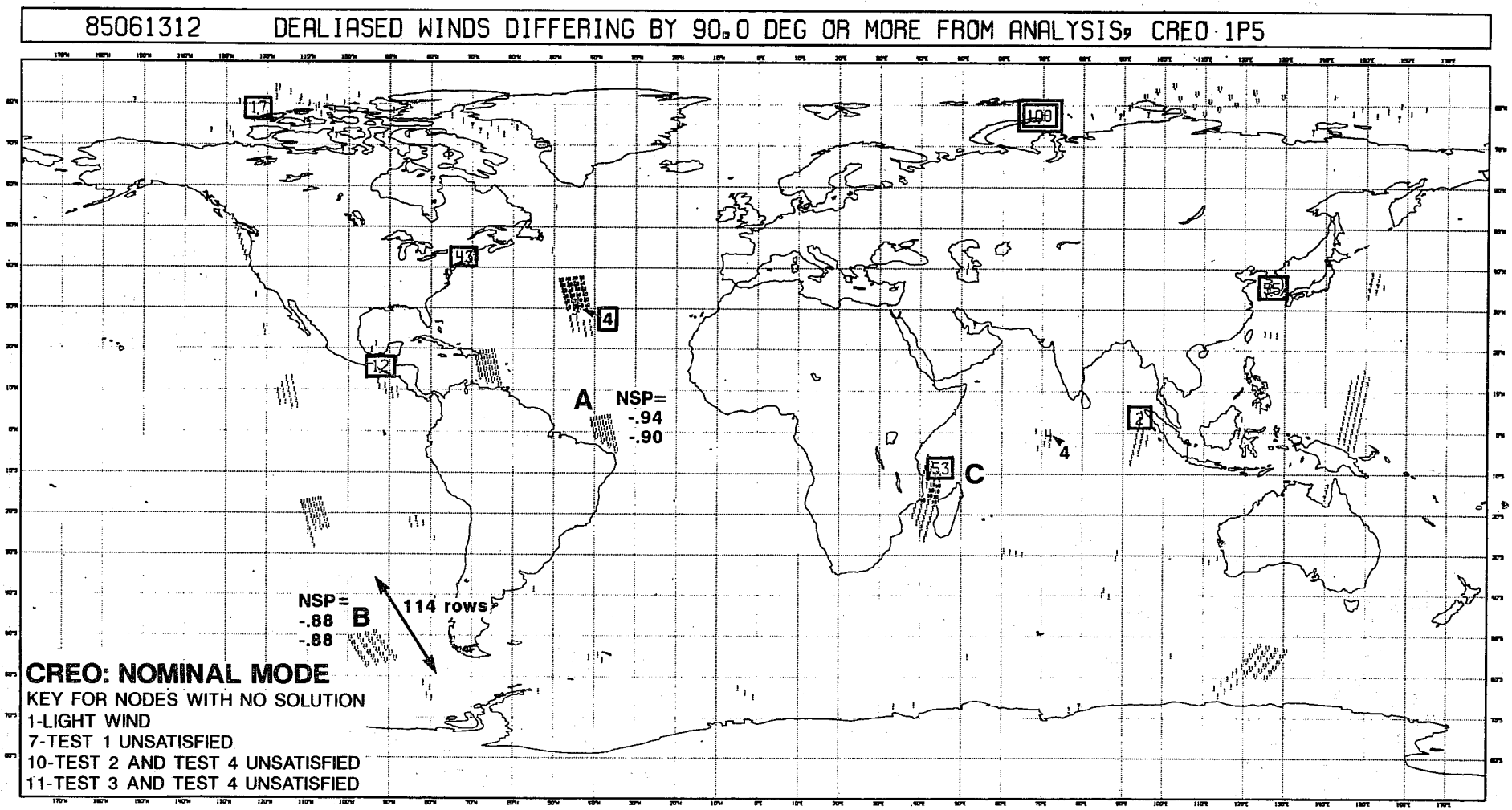

Fig. 6e: As for 6d, but when recourse can be made to a 48-hour forecast (whose directional errors are shown in fig. 6c). The number of regions where the ambiguity- removal software fails to make a return is now much smaller. The areas which are wrong on fig. 6d are still present, as the algorithm only calls for meteorological support when it is uncertain.

information to determine which is most consistent with the meteorological information. The field which in an area-averaged sense is most consistent with the forecast is then the selected field, provided the agreement is high enough. Otherwise, no solution is returned. (Although the algorithm works in packages of 19×19 cells, the tests are actually made over a number of these packages and hence the comparison is with the large scale information in the forecast). Fig. 6d shows the return after using the 48 hr forecast field as backup. Many of the previously low-confidence zones have now been 'confidently' and correctly dealiased. Some 7 zones still remain. Lest the reader think that the forecast was very good and that was the reason why the ambiguity could be removed so successfully by appeal to a forecast, the directional error in the 48 hour forecast is shown in fig. 6e. One can see a modest number of areas where the error is in the range 90° to 180° and many where it is in the range ~30–60°.

To give some feel for the 'numbers', when the algorithm is working in normal mode (i.e. has access to a 48 hr forecast) there were 77341 ocean cells of which 7841 were light winds so only 60,500 were eligible for dealiasing. Of these, only 217 were wrong (i.e. had directional errors >90°) but no solution was returned for ~5400 cells as the algorithm lacked confidence in those areas. Some improvements could be made to this algorithm to make more effective use of residual information but even without such improvements the algorithm performs quite well.

Recall however that a number of implicit assumptions have been made: that the model function is perfect, that the atmosphere has no structure below that of the analysis, that the σ^o return depends only on local processes and only on the wind, and that the antennae have no biases, none of which can be completely true, so further work is clearly needed to test this approach with more rigorous modelling of the possible errors.

An alternative approach to ambiguity removal is to load the evaluation of F with an additional contribution which measures the 'distance' between the trial solution and some 'prior' information and combine the retrieval and ambiguity processes (e.g. Schwenzfeger (1984)). The prior information could be a first guess from a meteorological forecast model, or information based on previously dealiased neighbouring solutions.

The two methods outlined above, that of CREO and that of Schwenzfeger, are both cell by cell techniques. In principle one could seek to dealias an extended region at once by broadening the definition of F to include many cells. Prior information,

other measurements and smoothness constraints can be used if so desired, but this is likely to be much more computationally expensive and probably not feasible for fast delivery products. A variational procedure (e.g. Hoffman 1982) could however be done at Weather Centres or off-line. At present it is not known if such an elaborate a scheme will be required.

4. Results using scatterometer data in an analysis forecast model.

4.1 Collocation of SASS data with ship data and model analyses

Because scatterometer data are boundary layer data it is likely that they will be difficult to use to maximum effect to correct the deep atmosphere. A number of attempts have been made with variable success. However, before discussing what the data can do for the analysis, we will first consider what the analysis can do for the data. In any versatile operational weather forecast system both processes are likely to be important: the scatterometer data to improve the analysis, the analysis and other data used to produce it, to quality control the scatterometer data. The data we will discuss are from SASS from the manually dealiased data set of September 6–17, 1978 referred to earlier. A fuller account of the work reported here can be found in Anderson *et al.* 1987.

Two main sets of assimilation experiments were performed, NOSASS and AESASS, the former being a control in which SASS data is appended to the analysis but not actively used in it. In the latter, the data is used to modify the analysis. The name AESASS is used to indicate that the data was obtained from AES CANADA. The dealiasing was performed manually by meteorological analysts from JPL, UCLA and AES. The data were assimilated into the ECMWF analysis/forecast model which was equivalent to that used operationally at the time (1986).

By combining the SASS data with all other measurements, it is also possible to compare (collocate) the SASS data with other observations. The results of such a collocation with ship data is shown in fig. 7a. It is clear that the two observing systems are not seeing the same thing. If one plots the mean SASS speed v ship speed then a clear bias is evident (fig. 7b), particularly at higher wind speeds. Such a bias is not new – it has been noticed by several authors although the magnitude appears to be larger here than has been noted in the past (Pierson 1981, Jones *et al.* 1982, Lame and Born 1982, Woiceshyn *et al.* 1986). Fig. 7a is capable of a different interpretation however. If one averaged ship data as a function of SASS wind speed one could conclude that ship

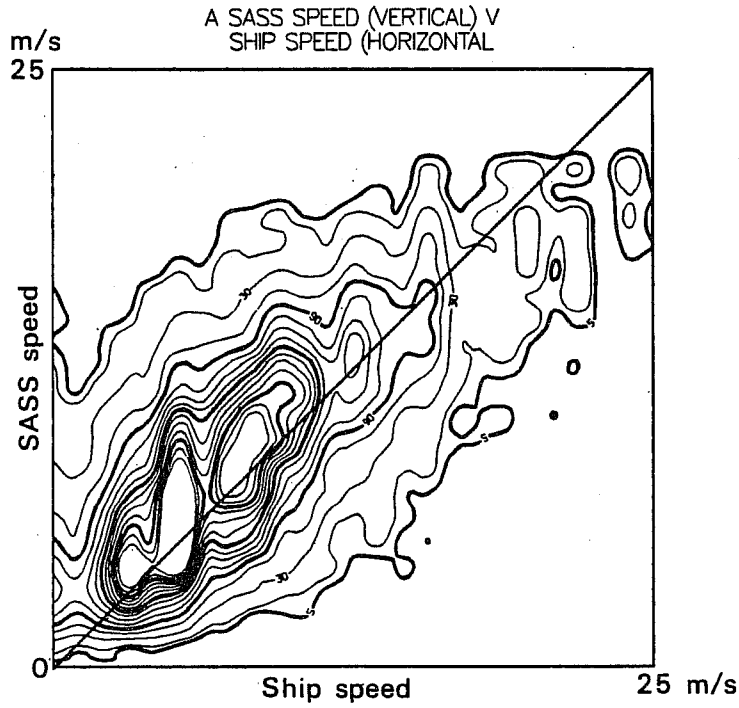

Fig. 7a: Contour plot of the number of collocations of SASS speeds with ship speeds, showing the large scatter in the collocated speeds. Much of this noise may come from noise in the ship measurements.

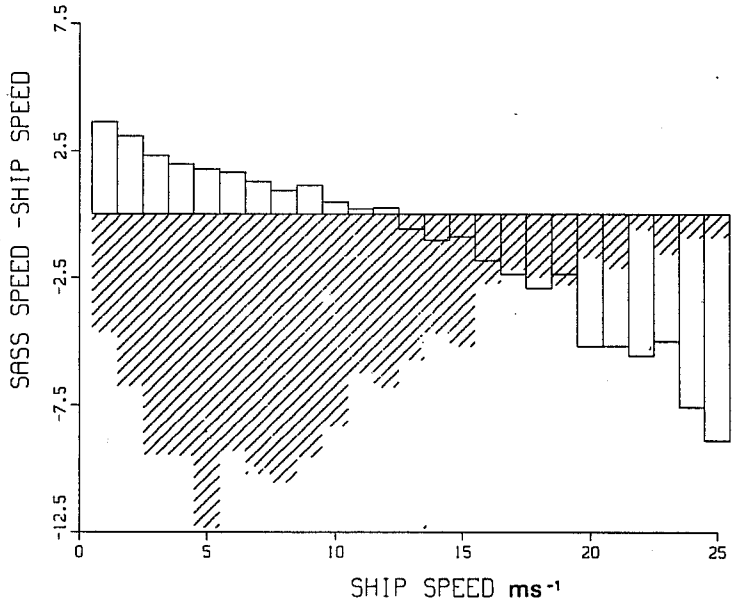

Fig. 7b: The mean speed difference between SASS speed and collocated ship speed plotted as a function of ship speed. The SASS speed is higher than ship speed at low ship speeds but substantially low compared with ship speeds at high ship speeds. The shading indicates the square root of the number of collocations. (-2.5 corresponds to 156, -5 to 625). Collocations are over the period from 3Z on the 6th September to 21Z on the 17th September 1978.

speeds are low relative to SASS speeds.

Since ship data are undoubtedly noisy, a cleaner comparison can be made between SASS data and model wind speed. Fig. 8 shows clearly that SASS data is biased low with respect to model wind speed at high wind speeds. This comparison is probably a bit worse than fig. 8 might indicate, for the SASS speed is supposed to apply at a height of 19.5m, the model winds are at 10m, and no correction for this height difference has been made. At low wind speeds, there is also a bias, but this time SASS speeds are high relative to the model or to ship wind speeds (fig. 7 and fig. 8). The result that SASS was biased high at low wind speeds was noted earlier by Woiceshyn *et al.* 1986. The explanation involves the way noisy data are handled at low wind speeds and a fuller discussion can be found in the above paper.

We now consider angular errors. In fig. 9 where the angular difference between SASS direction and ship direction is shown relative to ship direction, the scatter is large, particularly for wind directions lying between the beams. Some of this error undoubtedly results from dealiasing i.e. the wrong direction was selected from the possible choices, but part of the error comes from the retrieval process as seen in figs. 10 and 11 which show the frequency of occurrence of wind direction, measured relative to the space craft forward antennae, obtained from ship measurements (fig. 10) and from SASS measurements (fig. 11), angle. Since the ships do not know about the satellite, and are fairly widely spaced geographically (and hence sample many wind directions) one would expect an almost uniform distribution as fig. 10 shows. The distribution is not uniform however for directions obtained by SASS: there are significant peaks as shown in fig. 11. Further, these peaks are a function of incidence angle (not shown). At low incidence angles, wind directions along the beams are almost never sampled whereas at higher incidence angles they are frequent. Clearly this can not be correct. The fact that the distribution is a function of incidence angle suggests that the cause does not lie primarily with bad dealiasing. If a census of wind directions of all the aliases i.e. before the dealiasing stage is performed, a similar distribution results (fig. 11b) suggesting that there is a problem with the retrieval algorithm. Woiceshyn (Private Communication).

4.2 Effects of SASS data on analyses and forecasts

There have been a number of earlier studies to assess the impact of SASS scatterometer data on analyses, and forecasts made from these analyses. The first, (subjective),

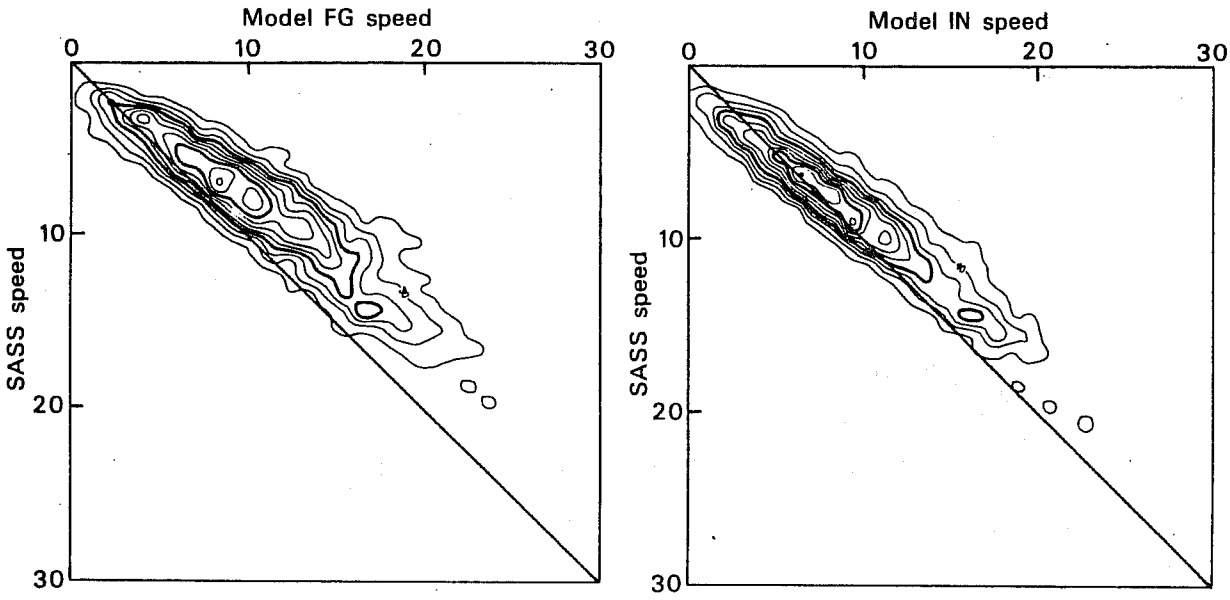

Fig. 8: Left-Contour histograms of model (FG) speed (across) v SASS speed (down). The axes range from 0 m/s to 30 m/s.

Right-Histograms of (IN) Analysis speed (across) v SASS speed (down). The axes range from 0 m/s to 30 m/s.

Only data for the six hour wind centred on 12Z on 11th September from the AE-SASS experiment are used. Comparison of left and right hand diagrams show the extent to which the FG has been altered by the SASS data. (Best seen by turning the diagram through 90°). There is considerably less noise in this figure than in fig. 7b suggesting that much of the scatter of fig.7b arises from noisy ship measurements.

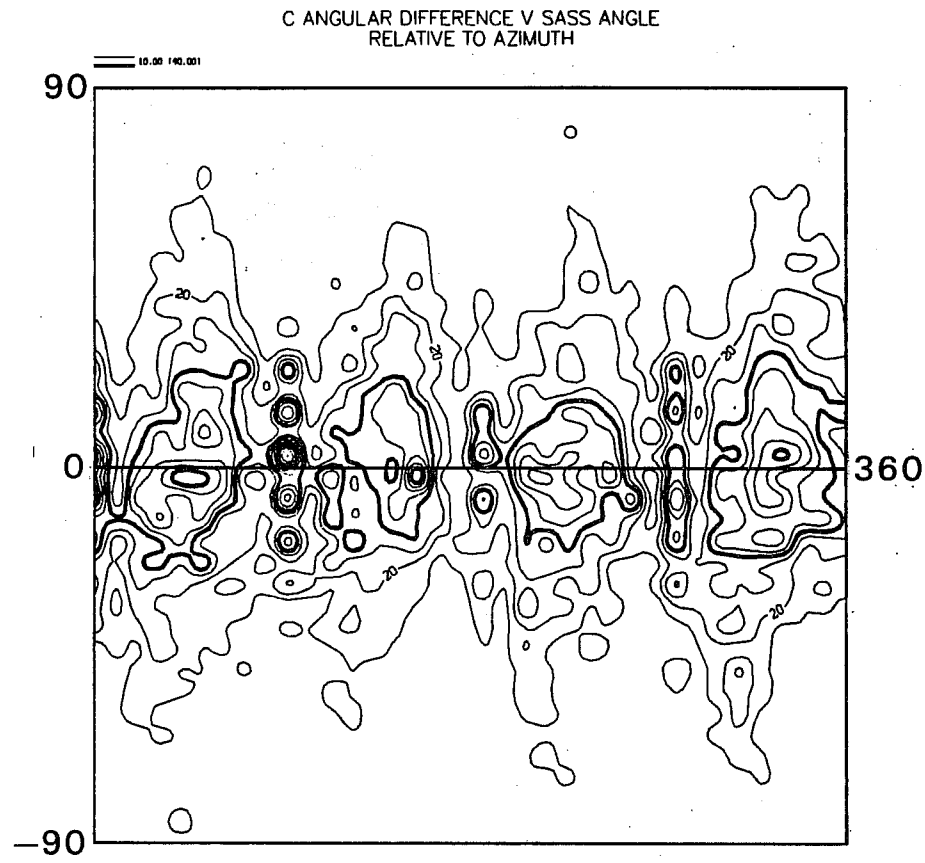

Fig. 9: Contour plot of the number of occurrences of the angular difference between wind directions as measured by ship and SASS, plotted as a function of SASS angle. The contour interval is 10, with a heavy contour every 20. Only winds with speeds greater than 5 ms^{-1} are used in this plot.

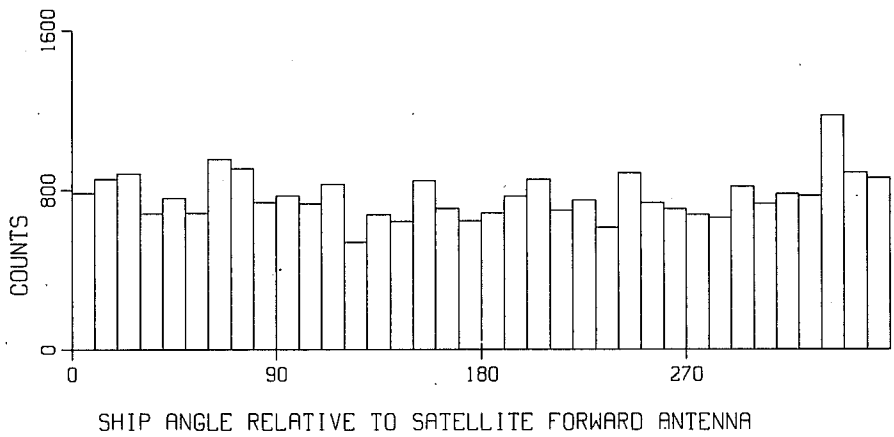

Fig. 10: No. of occurrences of a given wind direction as measured by ship but with the angular direction measured relative to the forward antenna of the spacecraft (azimuth).

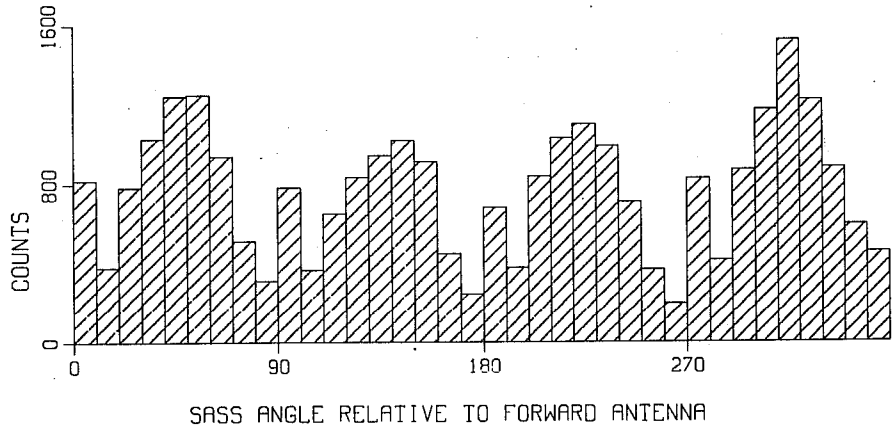

Fig. 11a: No. of occurrences of a given wind direction measured by SASS with the angular direction measured relative to the forward antenna of the spacecraft.

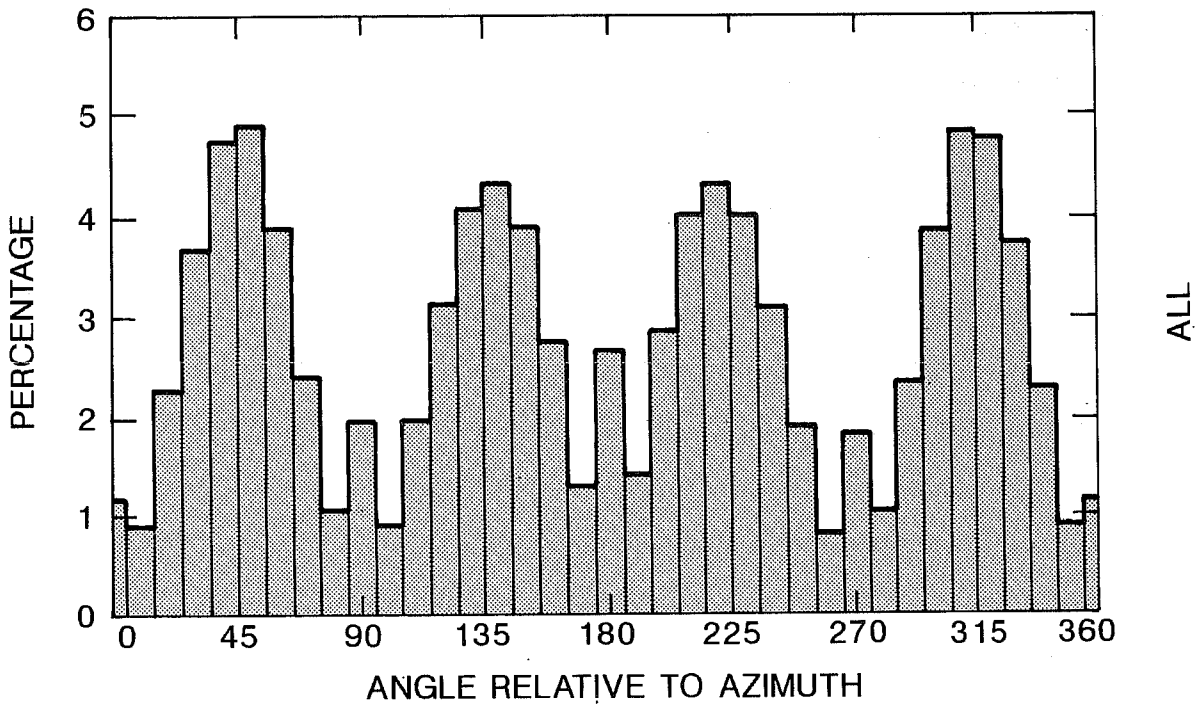

Fig. 11b: Frequency of occurrence of wind direction measured relative to the forward antenna of the spacecraft. The census is made from all alises following retrieval. The distribution is similar to that of fig. 11a, made after ambiguity removal, showing that the non uniform distribution is not a function of the dealiasing process.

studies were conducted manually (Peteherych, 1981a, b) and concluded that the inclusion of SASS data in the analyses resulted in more accurate placement of significant meteorological features such as storms and fronts. Further, in 75 percent of the case studies, improved forecasts resulted.

Cane *et al.* 1981, Atlas *et al.* 1984, Baker *et al.* 1984 and Yu and McPherson, 1984, have performed global numerical weather prediction experiments to study the impact of assimilation of single level boundary layer wind data on objective analyses and subsequent numerical forecasts. The results were mixed. Using simulated data, Cane *et al.* (1981) anticipated a beneficial impact from assimilating SASS data. This result, however, was not supported by Yu and McPherson (1984), Duffy *et al.* 1984, nor Baker *et al.* 1984. Baker *et al.,* assimilating SASS data from 00:00 on September 7 to 12:00 on September 13, concluded that the assimilation of SASS data had a negligible impact on Northern Hemisphere analyses and forecasts. In the Southern Hemisphere, SASS did have a significant impact on the analyses but it was not clear whether the impact was beneficial or not. Similar conclusions were reached by Duffy *et al.,* for the period of 7 to 13 September, 1978, and Yu and McPherson, in their more limited study of 16 to 17 July. The three above-cited studies used different forecast models: Yu and McPherson used the NMC 12 level spectral model, Baker *et al.* the GLAS 6 level model and Duffy *et al.* the 10 level NOGAP model. The structure of the boundary layer was different in these studies as was the horizontal resolution but in all cases it was, by present day standards, low, viz (2.4° lat, 3.75° long), (4° lat × 5° long), and (2.4° lat, 3° long) respectively. Further, the analysis may be done on a grid which is different from that of the model used to produce the first guess or forecast. The way the SASS data is used in the analysis is also a function of the analysis scheme e.g. whether a multivariate or univariate analysis is used or whether the influence of the SASS data is projected in the vertical, (as was the case in the Yu and McPherson study and perhaps to a lesser extent in the Duffy *et al.* case).

Before the SASS data can be used, one direction must be selected as the correct direction. All of the above studies used an objective method based on a model first guess field to select this direction which largely resulted in the direction closest to the model first guess being selected. Only limited information therefore was extracted from the SASS data: essentially speed.

More recently, Duffy and Atlas (1986) used a limited area, higher resolution model

(~100 km) to examine the impact of SASS on a specific synoptic event viz the QE-II storm, an example of explosive cyclogenesis (Anthes *et al.* 1983, Gyakum 1983). The SASS data was subjectively dealiased by Atlas (private communication). Contrary to the global studies, Duffy and Atlas (1986) found substantial positive impact as a result of assimilating SASS data, provided the data was projected in the vertical.

Since the impact of assimilation of any data type is a function of both the analysis scheme and forecast model used to provide the first guess, it is instructive to find what impact will be obtained in yet another model, in this case the ECMWF forecast model. This model and analysis scheme differ from those used in the earlier studies in that the global resolution is much higher and more elaborate schemes are used to combine the data and the model first guess to produce the analysis.

4.3 Description of the Analysis, forecast model and SASS dataset used

The model used in this study was equivalent to that used for operational forecasts in April 1986 and is described in Simmons *et al.* 1988, Tiedtke *et al.* 1988. It has higher vertical resolution (15 levels) than any of the above mentioned models, as well as having a reasonably elaborate boundary-layer scheme (Louis 1979). The lowest model level is at approximately 30 m. The horizontal resolution of the model which provides a first guess to the analysis or is used for forecasts is T106 (~100 km) and so is considerably higher than that used in previous global studies and comparable with that of the limited area forecast model used by Duffy and Atlas (1986). The analysis scheme, however, (described in Shaw *et al.* 1987) is at a lower resolution than the model (187.5 km). An optimum interpolation (O.I.) scheme is used to combine data and model first guess. The O.I. scheme acts as a filter (Hollingsworth, 1987), such that the analysis draws to the observations on the large scale but to the model first guess (F.G.) on the small scale. Small and large scale here are measured relative to the scale of the structure functions used to combine model FG and data. A representative scale is ~500 km in mid-latitudes.

The SASS data set used was produced manually by meteorological analysts from AES Canada, JPL and UCLA (Peteherych *et al.* 1981a, b) in a manner consistent with meteorological principles, satellite imagery and some surface reports. It should therefore contain directional as well as speed information. This directional information should be beneficial when dealiasing was done correctly but could be detrimental otherwise. The

period dealiased was 6–20 September 1978, though only the period to 18 September was used. The SASS data set was combined with the "FGGE Build-up year" data set created at NCM, Washington which includes ships reporting in delayed model. In the assimilation scheme SASS data is treated in much the same was as ship reports or Dribu reports. These reports are ascribed a height of 10 m. The model first guess at 10 m is calculated from the 30 m wind assuming a logarithmic boundary layer profile. A stability correction was not made to SASS data. The difference between a surface report and the model is then assigned to the 1000 mb level. There are 15 standard pressure levels used in the analysis, the lowest being at 1000 mb. Information on the statistics of short-range forecasts enters through the prediction error covariance function. This was taken to be the sum of terms which are the product of a vertical correlation and a horizontal correlation both of which are latitudinally variable. The vertical correlation is shown in fig. 12 for (a) the extratropics and (b) the tropics. The influence has dropped to one-third of its surface value by a height of 800 mb in the tropics but extends to 600 mb in the extratropics.

As illustrated in section 4.1, SASS data may have speed and angular errors arising from the retrieval as well as angular errors arising from ambiguity removal. The presence of these errors reduces the weight that can be given to the data in the analysis procedure. Presently the U and V components are assigned an error comparable with that given to ships viz 3.6 ms^{-1}.

4.4 Differences between AESASS and NOSASS analyses

In Fig. 13a, the difference between the analysis of the 1000 mb wind from the NOSASS and AESASS assimilation experiments is shown for 12UTC on September 9. North of 20° N, differences are usually small, but speed differences can be as large as 10 m/s (for example 12UTC on the 10th or 12UTC on the 16th). The spatial scale of the changes is usually quite small, despite the fact that the analysis will act to damp small-scale features. (Since this was our first experimentation with scatterometer data, no special steps were taken to adapt the analysis filter to the properties of the scatterometer data, but work is presently underway to improve the response of the analysis on small scales. It will also be essential to determine the spatial error correlation properties of the data, but for this study, the errors were taken to be uncorrelated). Some of the small scale structure evident in Fig. 13 could come from the model, being generated

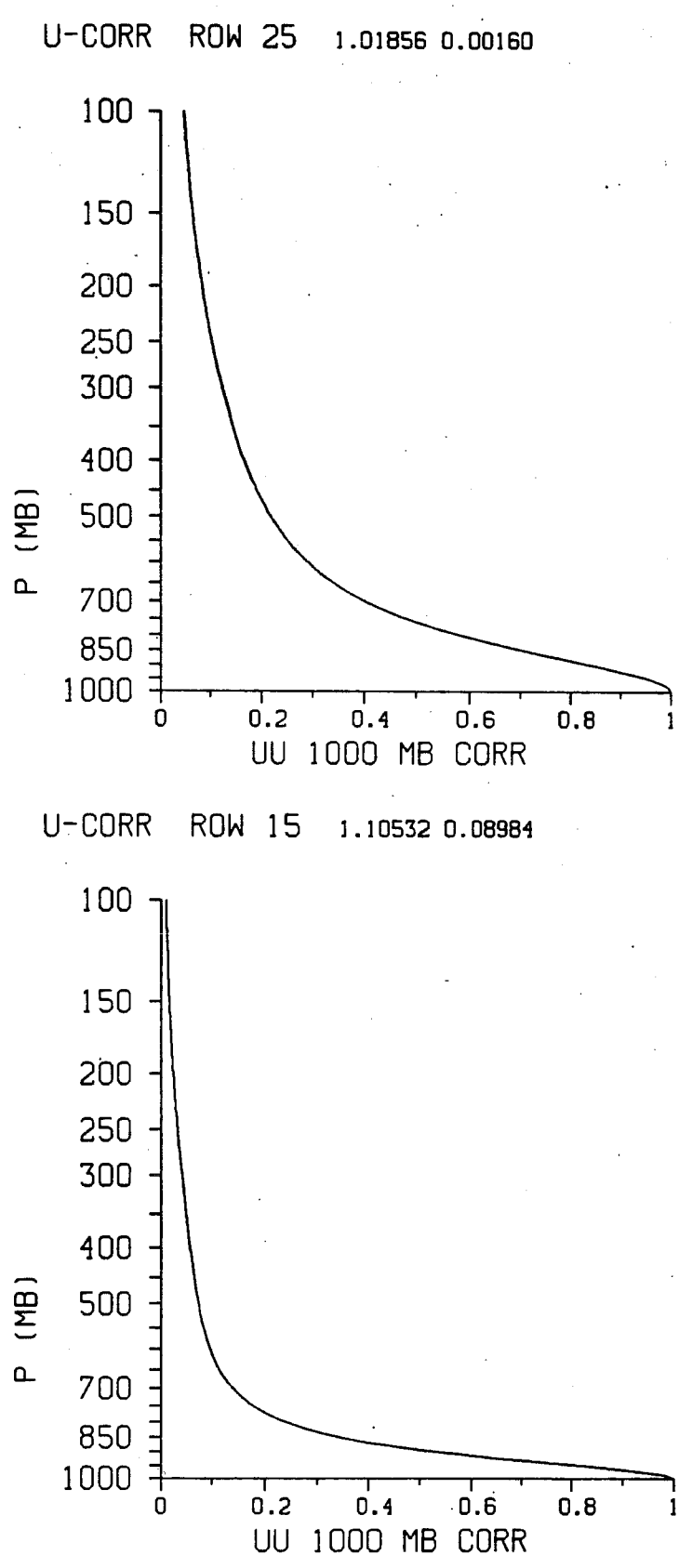

Fig. 12: Vertical correlation function used to extend vertically, the departure of the surface observation from the first guess for a) mid latitudes, b) tropics. From Per Undén, personal communication.

were probably more than 30 mb for the SASS forecast, taking a 100 km square central pressure of 955 mb at 12UTC on the 10th (Anthes *et al.* 1983).

In fig. 17, the 24 hour surface pressure forecast for 12Z on the 10th is plotted together with the verifying analysis in Fig. 18 for the AESASS experiments. Fig. 19 is a plot of the location of the QEII storm for the period 12UTC on the 9th to 12UTC on the 14th (a) as gauged by the German manual surface analysis, and (b) as determined from the forecast which started from the AESASS analysis of 12Z on the 9th. The position of the storm in the AESASS analyses is not shown but closely follows the German analyses. One can see from Fig. 19 that the ECMWF model forecast has modest errors in position. For example, at 00UTC on the 11th, the error is approximately 300 km.

In fig. 20 the central pressure from a number of sources is plotted for the period between 12UTC on the 9th and 00UTC on the 14th September. Not only is there a wide variation in the central pressure forecast by different models, there is a wide variation in the analysed values. In particular, both NMC and the German analysis probably underestimate the central pressure at 12UTC on the 10th, 00UTC on the 11th and 12UTC on the 11th. Pressures and positions of the QEII storm from the NOSASS analyses, and the forecast from the NOSASS analysis have not been plotted, as the NOSASS analyses hardly differ from the AESASS analyses and likewise the forecasts from these two analyses are very similar.

From Fig. 20, one can see that the forecast by the ECMWF model is not substantially better in amplitude than Duffy and Atlas at 00UTC on the 11th, but the position of the low is better forecast (Fig. 19). Unlike Duffy and Atlas, however we do not find SASS data to have had any important beneficial impact on the forecast. Duffy and Atlas find substantial changes in the low level analysed wind fields as a result of assimilating SASS. This is not the case for our analyses. It is interesting to speculate on why this difference. For SASS to have impact, it is necessary for the analysis without SASS (and forecasts from that analysis) to be deficient. The better the initial NOSASS analysis the less potential for impact for SASS. It would therefore appear that one interpretation of why Duffy and Atlas achieved impact and we did not was that their NOSASS analysis was worse than ours. One should note however that the ECMWF forecast, did not capture the rapid deepening between 00UTC and 12UTC on 10th September. Orlanski and Katzfey 1987 imply that higher resolution (~50 km) is necessary to capture rapid development, but Anthes *et al.* 1983 find little difference for the QEII storm when they

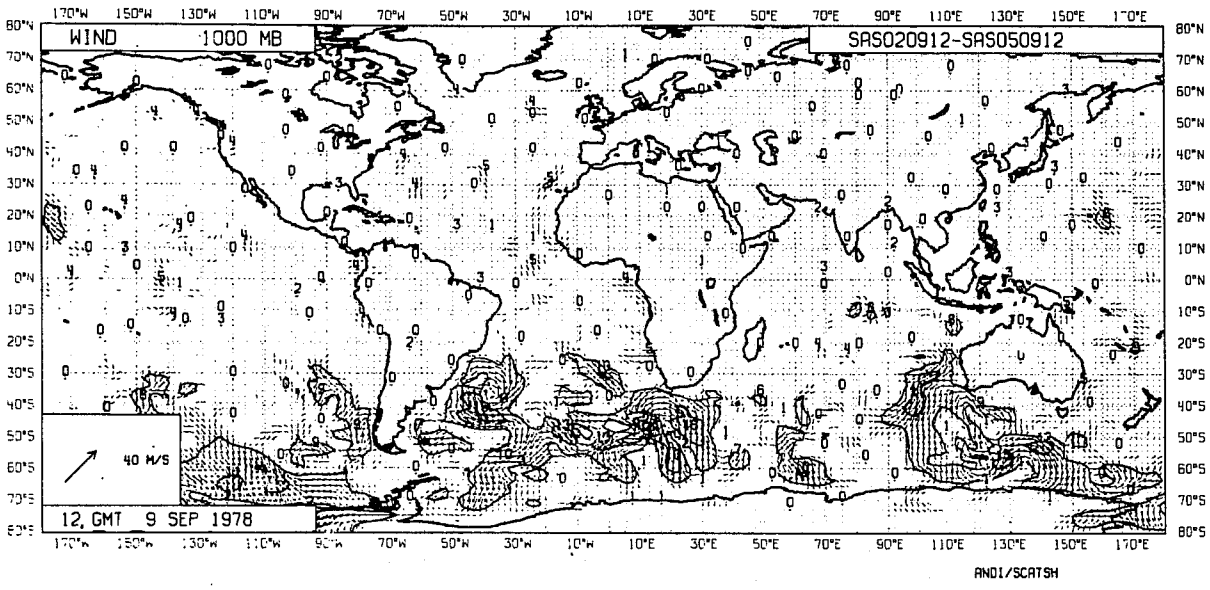

Fig. 13: Difference between analyses from the NOSASS and AESASS assimilations for winds at 1000 mb (upper) for 1200UT on Sept 9 1978. In the NH and tropics differences in wind are usually small but can be up to ~10m/s. The differences are usually small scale. In the SH, by contrast both the magnitude and spatial scale of the changes are larger. Contour interval for speed is 5 m/s.

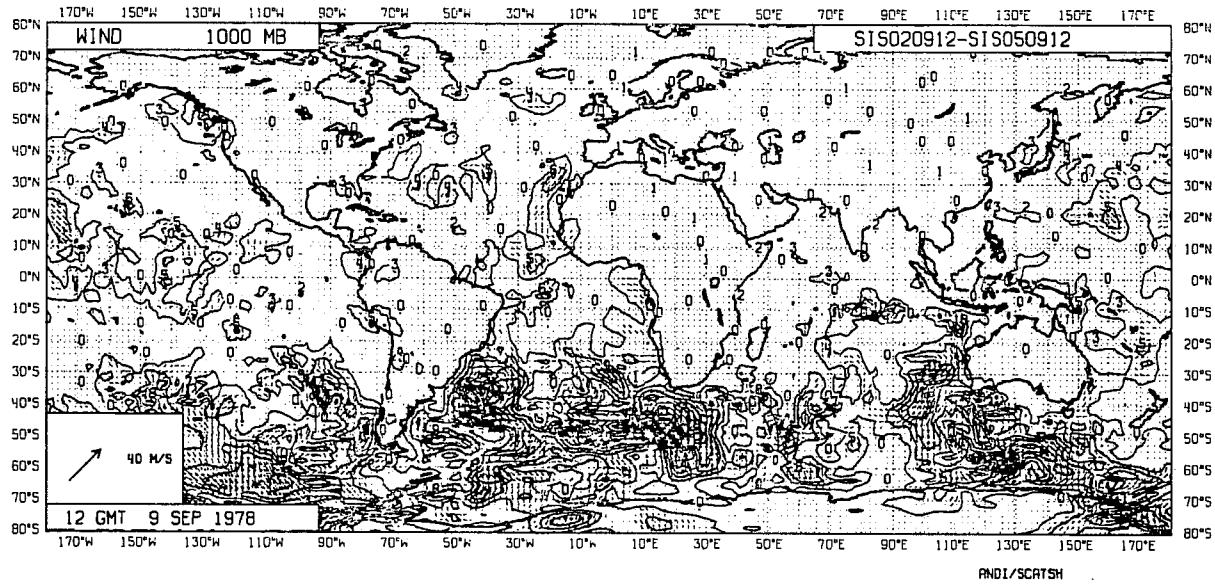

Fig. 14: Difference between the NOSASS and AESASS analyses for September 9 1978, 12GMT after initialisation showing that the changes introduced by the analyses survive initialisation (c.f. Fig. 13). The contour interval is 2 m/s for wind speed. Changes are being made in the Tropics of about 2–3 m/s.

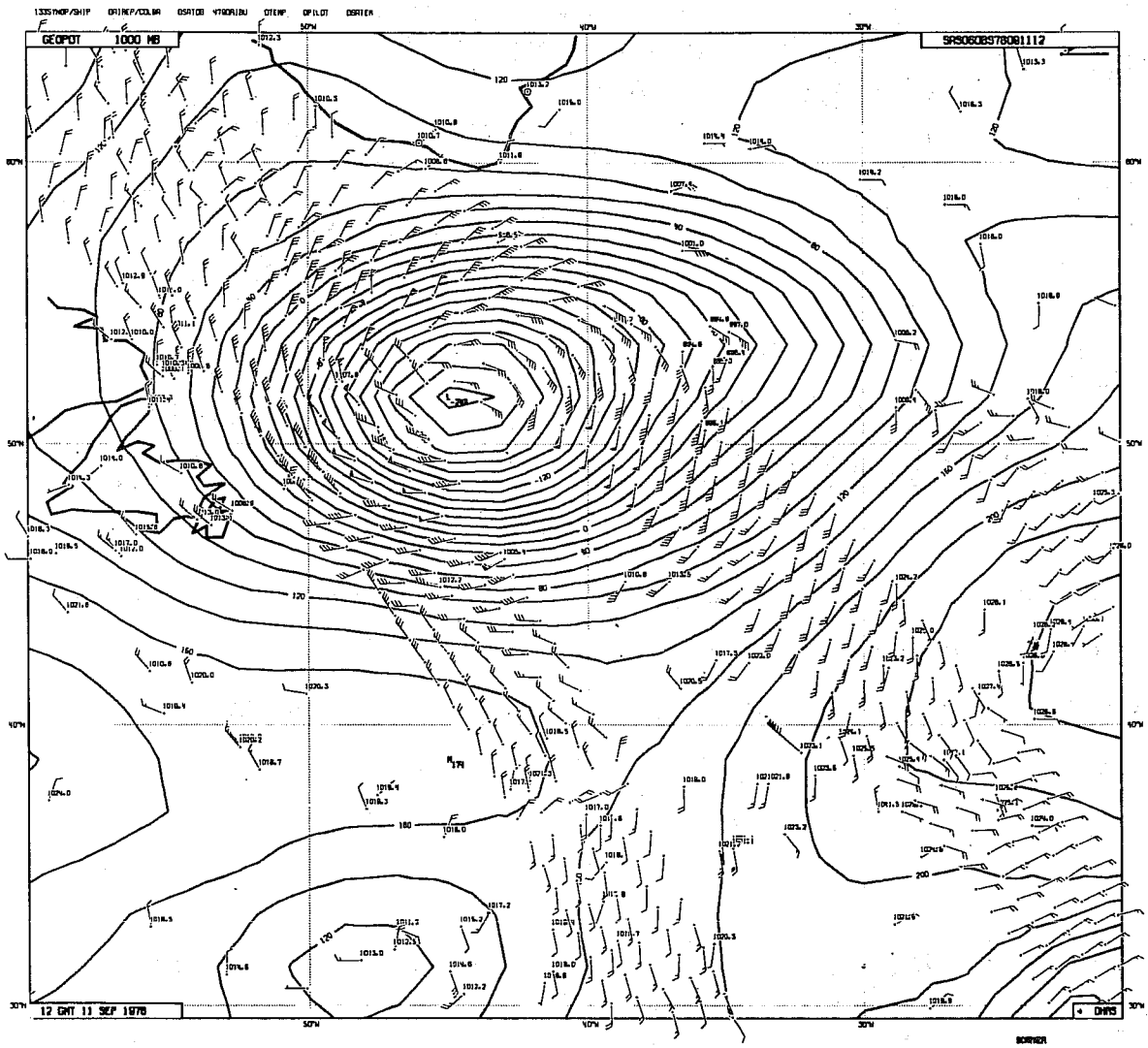

Fig. 15a: Analysis from the assimilation AESASS at 12UT on 11th September 1978. Superimposed on the contours of 1000 mb height are SASS and ship wind vectors. Ship reports show surface pressure in hPa.

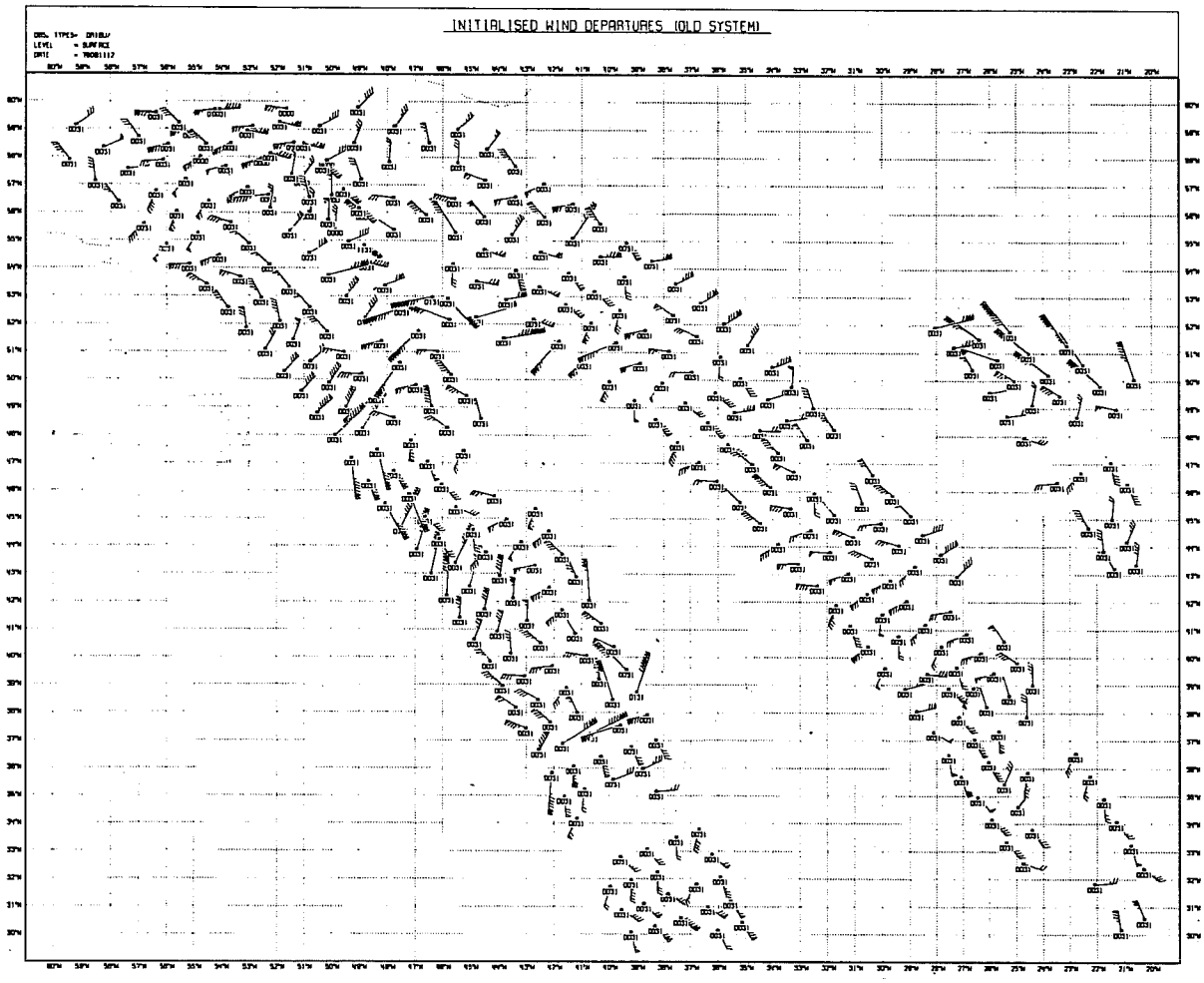

Fig. 15b: Differences between analysis and SASS measurements. A barb indicates 0.5 ms^{-1} and a fletch 2.5 ms^{-1}. The 4 digit code gives information on the extent to which the analysis software believes the vector wind and if it was assimilated or not. See text for details of the code.

illustrates the quality problems that can occur with any type of wind data.

Figure 16 shows a very sharp front in the SASS data near 160°W. This front is present in the model also but much less sharply defined. Present numerical models are not able to use such small scale information in the data to maximum effect since the analysis smooths out such sharp features, but progress in this direction is likely by the time data is available from forthcoming scatterometers.

4.6 Impact of SASS data on forecasts

A number of forecast experiments have been run from the AESASS and NOSASS analyses. The starting dates were partly chosen to include specific synoptic events such as the QEII and we will consider this storm here, as one study (Duffy and Atlas 1986) has found a beneficial impact of SASS data on a forecast for the QEII storm. This storm is of interest because of the failure of the NMC and Fleet Numerical Weather Centre (FNWC) operational forecast models to predict its intensification. It began as a shallow baroclinic disturbances approximately 100 km west of Cape Cod at 12Z on 9 September. During its movement out over the ocean, the low developed explosively, deepening by an estimated 60 mb in 24 hours to a minimum pressure of 945 mb at 12UTC on 10 September (Gyakum, 1983).

24 hour forecasts from 12UTC on 9 September by the NMC-LFMII model (horizontal resolution 190 km) gave a central pressure of 1000 mb, while the FNWC model (horizontal resolution 381 km) forecast a pressure of 999 mb. (Gyakum, 1983). The forecasts of the location of the centre of the storm and of the wind strength were likewise poor.

In their experiment without SASS data, Duffy and Atlas (1986) obtained results only slightly better than the NMC-LFMII model (the central pressure at 00Z on the 11th was 1000 mb with peak 'surface' winds, of 21 m/s). When SASS data was used, however, the forecast improved – the low intensified by 12 mb to 988 mb, with peak 'surface' winds of 37 m/s. Although assimilation of SASS data did lead to an improvement in the forecast, the forecast even with SASS was not especially good: there was a positional error of ~1000 km and a central pressure error of more than 10 mb (taking a 1000 km square average central pressure of ~975 mb for 00UTC on the 11th). The peak intensity of the storm occurred earlier (12Z on the 10th). Their forecast at 12UTC on the 10th was weaker (private communication) so that their pressure errors of that time

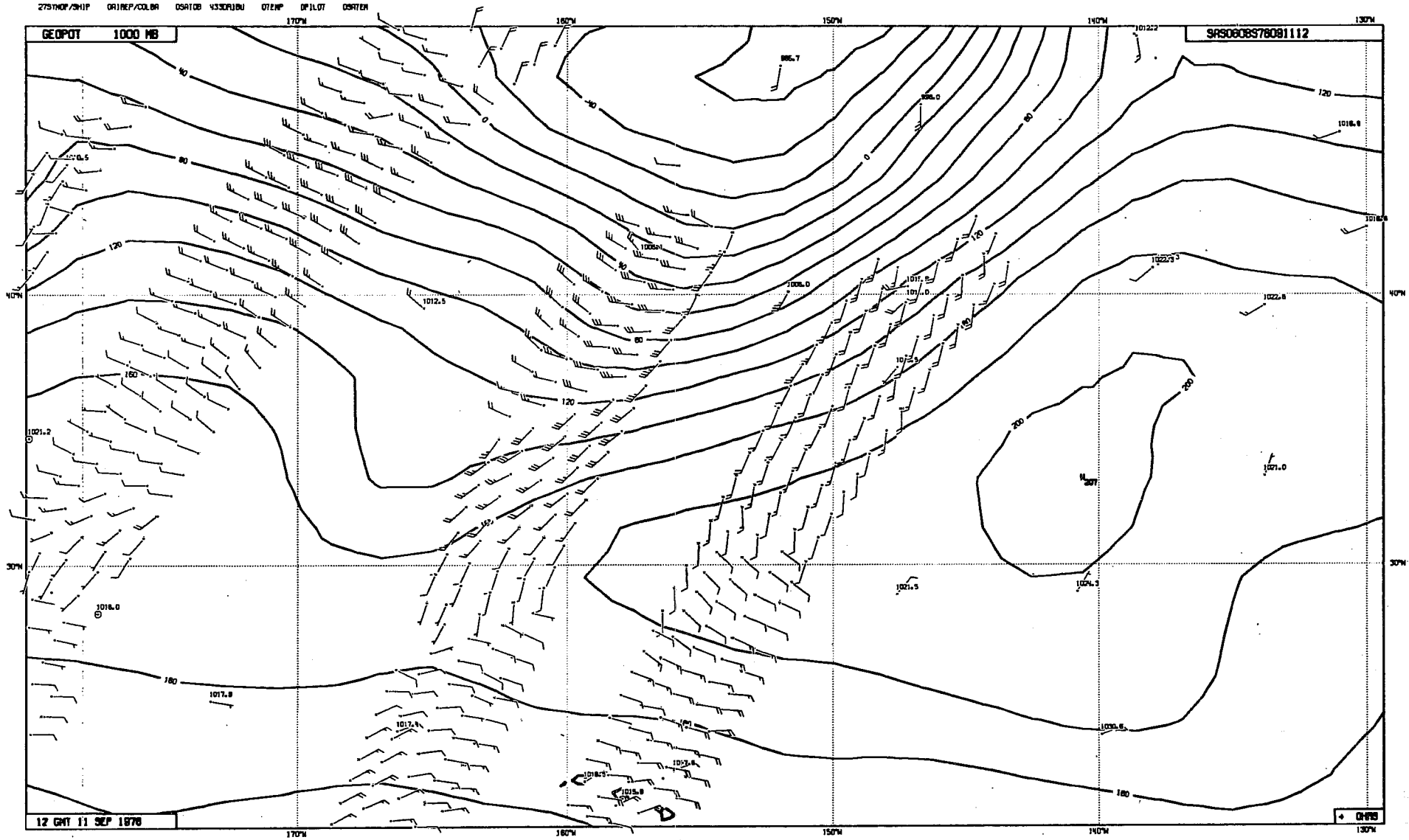

Fig. 16: As for fig. 15a but illustrating a sharp frontal feature well resolved by the SASS data. This front was poorly resolved both in the model first-guess and after analysis.

were probably more than 30 mb for the SASS forecast, taking a 100 km square central pressure of 955 mb at 12UTC on the 10th (Anthes *et al.* 1983).

In fig. 17, the 24 hour surface pressure forecast for 12Z on the 10th is plotted together with the verifying analysis in Fig. 18 for the AESASS experiments. Fig. 19 is a plot of the location of the QEII storm for the period 12UTC on the 9th to 12UTC on the 14th (a) as gauged by the German manual surface analysis, and (b) as determined from the forecast which started from the AESASS analysis of 12Z on the 9th. The position of the storm in the AESASS analyses is not shown but closely follows the German analyses. One can see from Fig. 19 that the ECMWF model forecast has modest errors in position. For example, at 00UTC on the 11th, the error is approximately 300 km.

In fig. 20 the central pressure from a number of sources is plotted for the period between 12UTC on the 9th and 00UTC on the 14th September. Not only is there a wide variation in the central pressure forecast by different models, there is a wide variation in the analysed values. In particular, both NMC and the German analysis probably underestimate the central pressure at 12UTC on the 10th, 00UTC on the 11th and 12UTC on the 11th. Pressures and positions of the QEII storm from the NOSASS analyses, and the forecast from the NOSASS analysis have not been plotted, as the NOSASS analyses hardly differ from the AESASS analyses and likewise the forecasts from these two analyses are very similar.

From Fig. 20, one can see that the forecast by the ECMWF model is not substantially better in amplitude than Duffy and Atlas at 00UTC on the 11th, but the position of the low is better forecast (Fig. 19). Unlike Duffy and Atlas, however we do not find SASS data to have had any important beneficial impact on the forecast. Duffy and Atlas find substantial changes in the low level analysed wind fields as a result of assimilating SASS. This is not the case for our analyses. It is interesting to speculate on why this difference. For SASS to have impact, it is necessary for the analysis without SASS (and forecasts from that analysis) to be deficient. The better the initial NOSASS analysis the less potential for impact for SASS. It would therefore appear that one interpretation of why Duffy and Atlas achieved impact and we did not was that their NOSASS analysis was worse than ours. One should note however that the ECMWF forecast, did not capture the rapid deepening between 00UTC and 12UTC on 10th September. Orlanski and Katzfey 1987 imply that higher resolution ($\sim$50 km) is necessary to capture rapid development, but Anthes *et al.* 1983 find little difference for the QEII storm when they

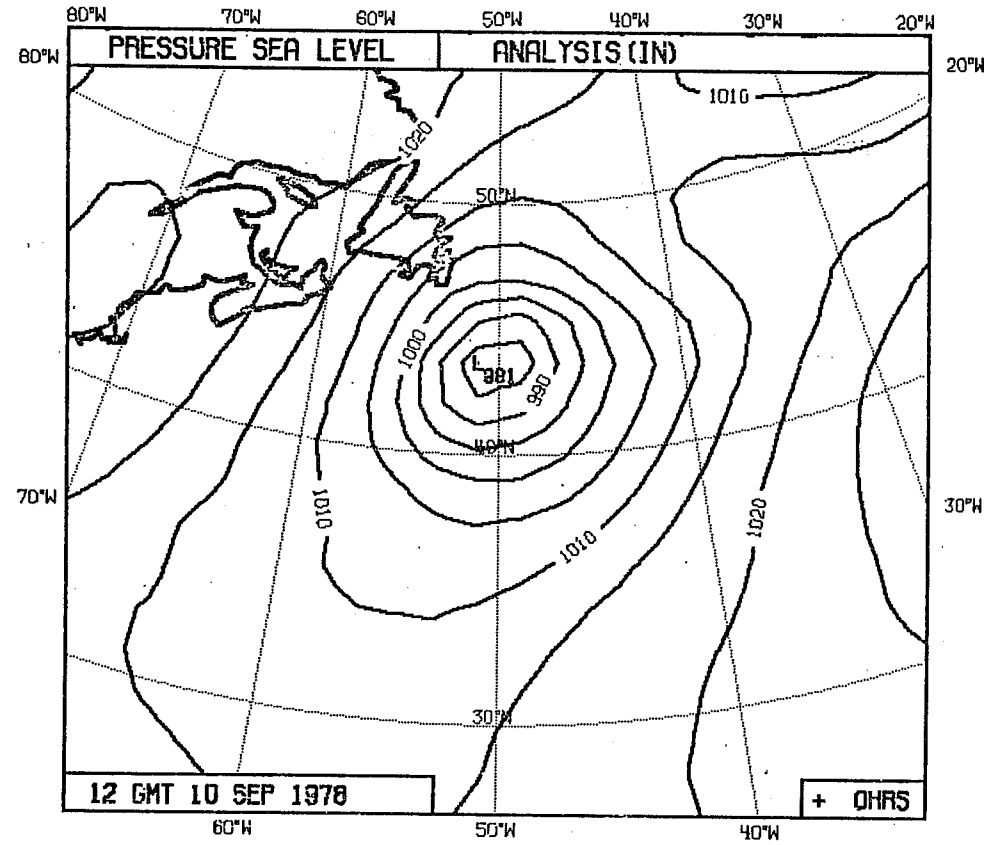

Fig. 17: Verifying analysis for 12Z on Sept 10 1978.

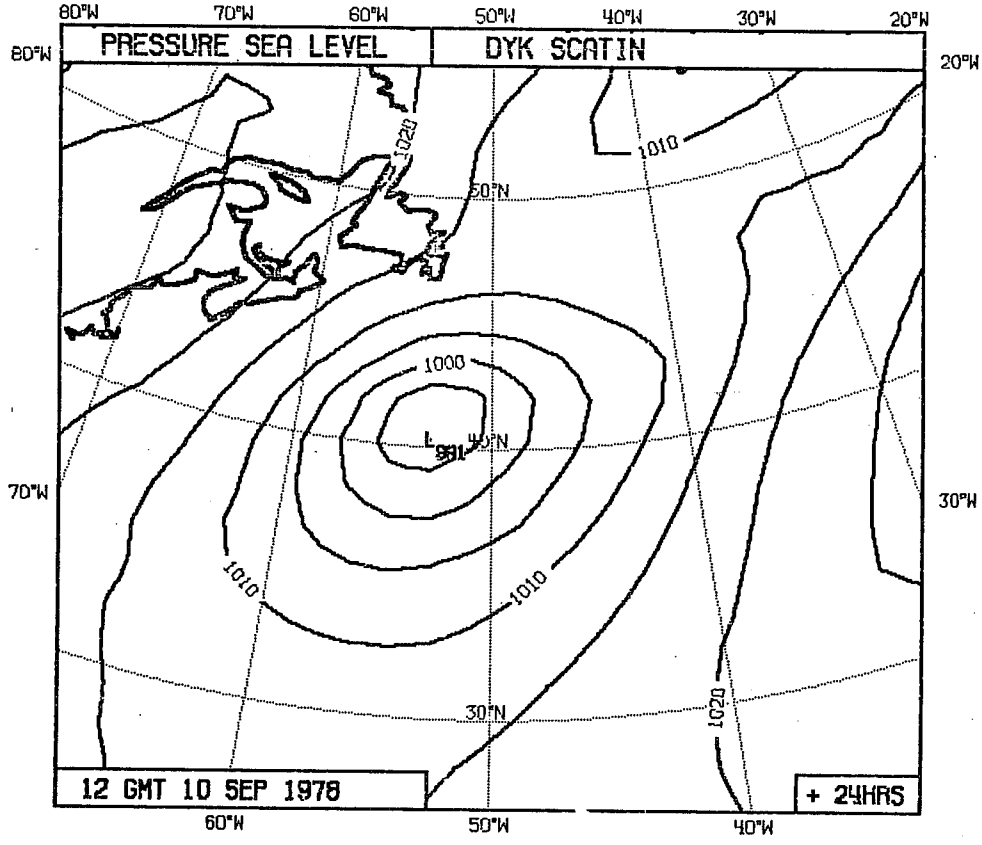

Fig. 18: 24–hour surface pressure forecast for 12Z on Sept 10 started from the AESASS analysis.

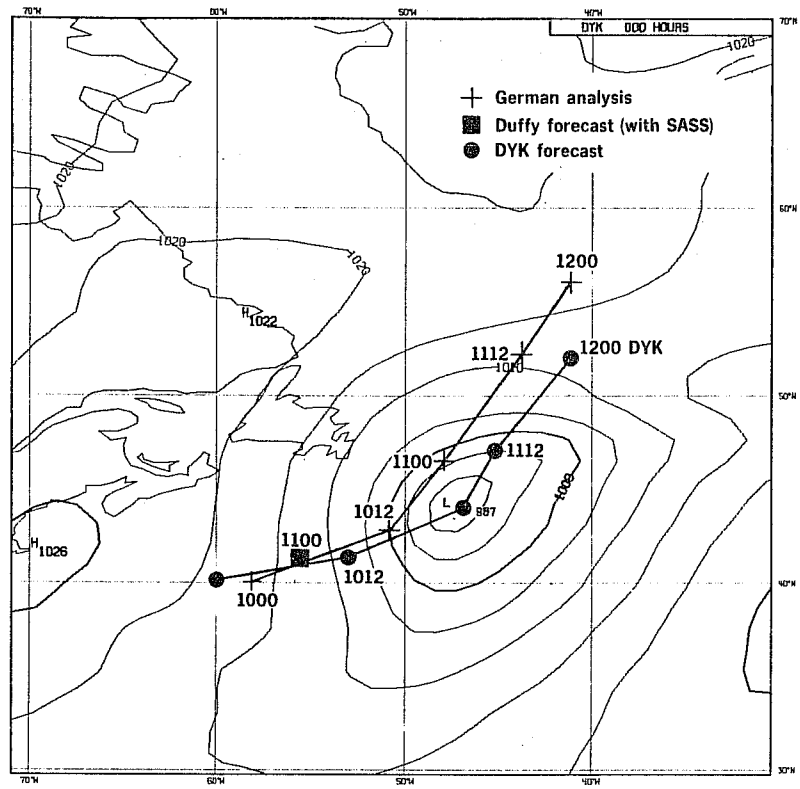

Fig. 19: Track of QEII storm from AESASS forecast and German analyses. The location of the QEII storm as forecast by Duffy *et al.* at 00 UHT on 11 September is plotted. Contours of height of 1000 mb surface for this time are shown for the AESASS forecast.

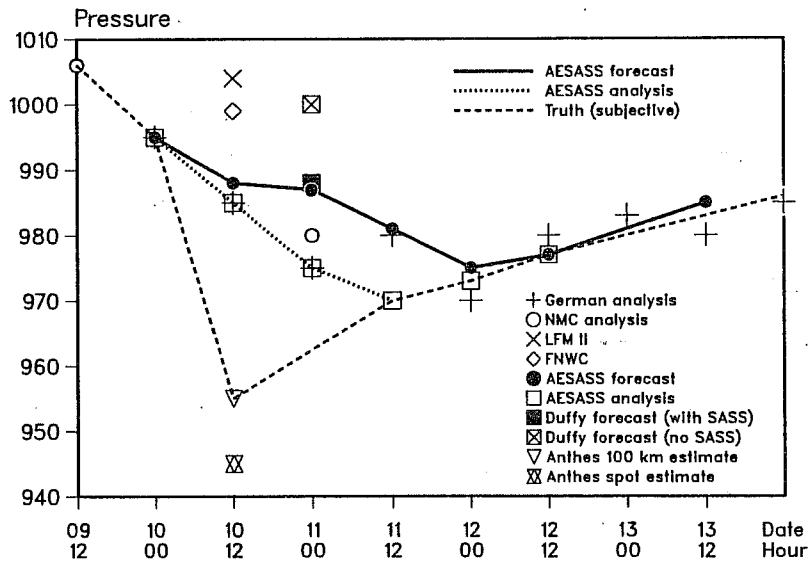

Fig. 20: Time evolution of surface pressure as gauged by a number of analyses or forecasts. No forecast reproduces the rapid deeping between 00 UHT and 12 UHT on the 10th September.

change their resolution from 100 km to 50 km, and in the 100 km case produce a more intense system than we do (see their fig. 1). Another possible reason for the difference between the present results and those of Duffy and Atlas is that the SASS data sets used were different. We used the JPL-AES-UCLA produced fields, while Duffy and Atlas used fields dealiased by Atlas (personal communication).

More recently Atlas (personal communication) has used a higher resolution global version of the GLA model ($2.5 \times 2.5°$). The forecast for the QEII storm with this model is better than that produced by the ECMWF model, both in terms of storm position and intensity. Further, Atlas is still able to show a positive impact from using SASS data so countering the argument given above for why there was little impact with the ECMWF model. The impact from SASS is not very large ($\sim$3 mb improvement in the forecast intensity) but encouraging. One might not expect over-large impact on forecasts, for at the time of the analysis, the QEII storm was not developed and according to Gyakum its inception was not especially related to the ocean. As we learn to use this data, one might anticipate that the impact will be greater on maritime storms than those which develop largely over land.

While the experience with the ECMWF system is rather negative in the sense that SASS data had little impact on N.H. analyses and forecasts, this should not be taken to imply that scatterometer data is of little use. But rather that one does not yet know how to use them to best effect. Many aspects of the assimilation system will need refinement: the analysis should be at the same resolution as the forecast model: the spatial structure functions in the analysis should be of higher resolution to capitalise on the high resolution of the data. Further, if one can be more confident of the quality of the wind directions and speeds, greater weight could be given to the scatterometer data and hence greater impact anticipated. More adaptive structure functions in the vertical (Bengtsson 1978) are needed in order to project the data more sensitively in the vertical.

References

Anderson, D.L.T., A. Hollingsworth, S. Uppala, P. Woiceshyn, 1987: "A study of the feasibility of using sea and wind information from the ERS-1 satellite. ECMWF Publication *120pp.*

Anthes, R.A., Y.-H. Kuo, and J.R. Gyakum, 1983: "Numerical simulations of a case of explosive marine cyclogenesis," Mon. Wea. Rev., **111**, *1174–1188.*

Atlas, D., R.C. Beal, R.A. Brown, P. DeMey, R.K. Moore, C.G. Rapley, and C.T. Swift, 1986: "Problems and future directions in remote sensing of the oceans and the troposphere: a workshop report", J. Geophys. Res., **91**, *2525–2548.*

Atlas, R., W.E. Baker, E. Kalnay, M. Halem, P. Woiceshyn and S. Peteherych, 1984: "The impact of scatterometer wind data on global weather forecasting," Proceedings of the URSI Commission F Symposium and Workshop, Shoresch, Israel, May 14–23, 1984, NASA Conf. Publ. **CP-2303**, *567–573.*

Aune, R.M. and T.T. Warner, 1983: "Impact of SEASAT wind data on a statistically initialized numerical model," paper presented at the Sixth Conf. on Numerical Weather Prediction, Amer. Meteorol. Soc., Omaha, Nebr.

Baker, W.E., R. Atlas, E. Kalnay, M. Halem, P.M. Woiceshyn, S. Peteherych, and D. Edelmann, 1984: "Large-scale analysis and forecasting experiments with wind data from SEASAT A scatterometer," J. Geophys. Res., **89**, *4927–4936.*

Bengtsson, L. 1978: Growth rate and vertical propagation of the initial error in baroclinic models. **30**, *323–334.*

Cane, M.A., V. Cardone, M. Halern, and I. Halberstorm, 1981: "On the sensitivity of numerical weather prediction to remotely sensed marine surface wind data: a simulation study". J. Geophys. Res. **86**, *8093–8106.*

Cavanie, A. and P. Lecomte, 1986: "Study of a method to dealias winds from ERS-1 data". ESA contract No. 6874/87/GP-I/Sc.

Duffy, D.G., R. Atlas, T. Rosmond, E. Barker, and R. Rosenberg, 1984: "The impact of SEASAT scatterometer winds on the Navy's operational model," J. Geophys. Res., **89**, *7238–7244.*

Duffy, D.G., and R. Atlas, 1986: "The impact of SEASAT-A scatterometer data on the numerical prediction of the Queen Elizabeth II storm," J. Geophys. Res., **91**, *2241–2248.*

Graham, R., D. Anderson and A. Hollingsworth, 1988: "Evaluation tests of ERS-1 wind extraction and ambiguity removal algorithms". ECMWF Publication.

Gyakum, J.R., 1983: "On the evolution of the QE II Storm. I: Synoptic Aspects," Mon. Wea. Rev., **111**, *1137–1155.*

Harlan, J. Jr., and J.J. O'Brien, 1986: Assimilation of Scatterometer Winds Into Surface Pressure Fields Using a Variational Method. Journal of Geophysical Research, **91**, *7816–7836.*

Hoffman, R.N., 1982: "Sasswind ambiguity removal by direct minimiation. Mon. Wea. Rev. **110**, *434–445.*

Hollingsworth, A., 1987: "Objective Analysis for Numerical Weather Prediction". J. Met. Soc. Jap., (in press).

Jones, W.L., L.C. Schroeder, D.H. Boggs, E.M. Bracalente, R.A. Brown, G.J. Dome, W.J. Pierson and F.J. Wentz, 1982: "The SEASAT-A satellite scatterometer: the geophysical evaluation of remotely sensed wind vectors over the ocean," J. Geophys. Res., bf 87, *3297–3317.*

Lame, D.B., and G.H. Born, 1982: "SEASAT measurement system evaluation: achievements and limitations," J. Geophys. Res., **87**, *3175–3178*

Long, A.E., 1986: "Towards a C-band radar sea-echo model for the ERS-1 scatterometer". Proceedings of the conference on spectral signatures of objects in remote sensing. Les Arcs December 1985, Paris ESA No. SP-247.

Louis, J.R., 1979: "A parametric model of vertical eddy fluxes in the atmosphere". Bound. Layer Meteor. **17**, *187–202.*

Orlanski, I., and J.J. Katzfey, 1987: "Sensitivity of model simulations for a coastal cyclone", To appear in Mon. Wea. Rev.

Peteherych, S., P.M. Woiceshyn, W. Appleby, L. Chu, J. Spagnol, and J.E. Overland, 1981: "High resolution marine meteorological analysis utilizing SEASAT," in Oceanography from Space, ed. J.F.R. Gower, Marine Science, **Vol. 13**, Plenum Press, N.Y., *pp. 581–586.*

Peteherych, S., P.M. Woiceshyn, W. Appleby, L. Chu, J. Spagnol, and J.E. Overland, 1981: "Applications of SEASAT scatterometer wind measurements for operational weather forecasting", in Final Report – An Evaluation of the Utility of Seasat Data to Ocean Industries, Vol. III, ed. Hubert, W., B.P. Miller and D. Montgomery, JPL Int. Doc. 622–225, Jet Propulsion Laboratory, Pasadena, California.

Phillips, O.M., 1985: Spectral and statistical properties of the equilibrium range in wind generated gravity waves. J. Fluid Meds. **156**, *505–531.*

Pierson, W.T., 1981: "Winds over the ocean measured by scatterometer. In Oceanography from Space. J. Gower Ed., Plenum, *978pp.*

Schwenzfeger, K., 1985: "Algorithm for wind scatterometer data analysis – ambiguity suppression". Proceedings of a conference on the use of satellite data in climate models. Alpbach ESA-SP244.

Shaw, D.B., P. Lönnberg, A. Hollingsworth and P. Unden, 1987: The 1984/85 revisions of the ECMWF assimilation system. Quart. J. Roy. Meteor. Soc. **113**, *551–567.*

Simmons, A.J., D.M. Burridge, M. Jarvald, C. Girard and W. Wergen, 1989: Met. and Atm. Physics. In press.

Tiedke, M., W. Heckley and T. Slingo, 1988: "Tropical forecasting at ECMWF: The influence of physical parameterisation on the mean structure of forecasts and analyses". Q.J.R.M.S. **114**, *639–665.*

Woiceshyn, P.M., M.G. Wurtele, D.H. Boggs, L.F. McGoldrick, and S. Peteherych, 1986: "The necessity for a new parameterisation of an empirical model for wind/ocean scatterometry," J. Geophys. Res., **91**, *2273–2288.*

Woiceshyn, P.M., M.G. Wurtele, M. Ghil, and D.H. Boggs, 1986: "Global Meteorological Research with scatterometer wind data". A proposal to NASA.

Wurtele, M.G., P.M. Woiceshyn, S. Peteherych, M. Borowski and W.S. Appleby, 1982: "Wind direction alias removal studies of SEASAT scatterometer-derived wind fields," J. Geophys. Res., **87**, *3365–3377.*

Yu, T.-W., and R.D. McPherson, 1984: "Global data assimilation experiments with scatterometer winds from SEASAT-A," Mon. Wea. Rev., **112**, *368–376.*